Construction of a Diesel Engine Test Stand and a Crank Angle Based Heat Release Model

by

Taylor Jennings Wingo

A thesis submitted to the Graduate Faculty of
Auburn University
in partial fulfillment of the
requirements for the Degree of
Master of Science

Auburn, Alabama
December 12, 2011

Approved by:

Song-Yul Choe, Chair, Professor of Mechanical Engineering
Timothy McDonald, Professor of Biosystems Engineering
David Beale, Professor of Mechanical Engineering

Abstract

A test stand for a light duty diesel engine was constructed and used to measure both mean and crank angle based engine operating parameters. The test stand features a 1.1L Hyundai CRDi turbo-diesel engine, a Land and Sea Dynamometer, and requisite instrumentation. Measured operating parameters include temperature (ECT, oil, EGT, intake air), mass air flow, manifold pressure, air-fuel ratio, engine speed, and load torque. Crank angle resolved measurements include in-cylinder pressure, injector current, and fuel-rail pressure. In-cylinder pressure traces were used to calculate rate of heat release (ROHR) curves for specific engine loads and speeds. A heat release estimation model was then calibrated using the experimental ROHR curves and expanded to handle multiple fuel injections per cycle. A comprehensive engine model was created that includes estimation of heat release, heat transfer to the surrounding cylinder, thermodynamic properties of the cylinder, engine geometry, and input fuel and air quantities. The model provides the pressure, temperature, gross heat release and heat transfer rate, cumulative gross heat release and heat loss on a crank angle basis. Other model outputs including indicated work, indicated torque, brake torque, and indicated specific fuel consumption (ISFC) per cycle were calculated and compared with dynamometer results.

Acknowledgements

I am grateful for the love and support of my parents, Steve and Linda Wingo. I would not have been able to complete this project without their encouragement. My sincere appreciation goes to Blake Thames for his integral part in completing the engine test stand, and Russell Green, my classmate and friend, for his advice and judgment in class and throughout the project. I would like to acknowledge the help of Dr. Song-Yul Choe, Dr. Timothy McDonald, and Dr. David Beale on my committee. I am appreciative of the opportunity to learn more about diesel engines and the guidance that Dr. Choe has given me over the years.

Table of Contents

List of Figures

List of Tables

List of Terms

Abbreviations and Acryonyms

A/F	air to fuel ratio
AFBR	apparent fuel burning rate
AHRR	apparent heat release rate
BDC	bottom dead center
CA	crank angle
CAN-bus	controller area network
CIDI	compression ignition direct injection
CRDi	common rail direct fuel injection
ECT	engine coolant temperature
ECU	engine control unit
EGR	exhaust gas recirculation
EGT	exhaust gas temperature
EOI	end of injection
FIPC	fuel injection per cycle
GPM	gallons per minute
HPFP	high pressure fuel pump
IAC	idle air control
IAT	intake air temperature
INJ	fuel injector

IMEP	indicated mean effective pressure
ISFC	indicated specific fuel consumption
IMAP	intake manifold pressure
IVC	intake valve close
MAF	mass air flow
P-V	pressure vs. volume diagram
PW	pulse width
PWM	pulse width modulation
RMS	root mean square
ROHR	rate of heat release
SOC	start of combustion
SOI	start of injection
TDC	top dead center
VGT	variable geometric turbo

Equation Symbols

a	Watson shape parameter coefficient
A	combustion chamber surface area
A_{ch}	cylinder head combustion chamber surface area
A_n	injector nozzle minimum area
A_p	piston crown surface area
β	Watson proportionality factor
b	Watson shape parameter coefficient
B	cylinder bore
c	Watson shape parameter coefficient

c_A	Weibe combustion efficiency coefficient
c_B	Weibe shape factor coefficient
c_v	specific heat at constant volume
C	Woschni heat transfer calibration constant
C_{mot}	average cylinder gas velocity empirical calibration parameter
C_{comb}	average cylinder combustion empirical calibration parameter
C_1	Watson pre-mixed peak timing shape parameter
C_2	Watson pre-mixed peak slope shape parameter
C_3	Watson diffusion controlled burn rate shape parameter
C_4	Watson diffusion controlled timing shape parameter
C_D	fuel injector discharge coefficient
C_R	radiation mode heat transfer calibration constant
ε	difference between estimated and test parameters
γ	ratio of constant pressure specific heat to constant volume specific heat
h	specific enthalpy
h_f	enthalpy of fuel
h_g	heat transfer coefficient
k_c	thermal conductivity for convective heat transfer coefficient
K_R	radiation mode heat transfer calibration constant
L_c	characteristic length for convective heat transfer coefficient
m	mass of the working fluid
m_b	burned fuel mass
m_d	diffusion-controlled phase burned fuel mass

$m_{f,inj}$	mass of injected fuel
m_p	pre-mixed phase burned fuel mass
M_b	Weibe burned gas fraction
υ	characteristic speed
υ_{pis}	mean piston speed
N	engine speed [RPM]
φ	overall equivalence ratio
φ_{ig}	trapped equivalence ratio
P	cylinder pressure
P_r	fuel rail pressure
Pr	Prandtl number
Q	heat transfer
Q_{ch}	gross heat release
Q_{LHV}	lower heating value
Q_n	net heat release
Q_{ht}	heat loss to combustion chamber cylinder walls
Q_{LHV}	heating value of fuel
ρ_f	fuel density
r_c	compression ratio
R	compression ratio
R_v	rod to stroke ratio
Re	Reynolds number
σ	Stefan-Boltzmann constant

τ	dimensionless time from SOC
τ_{id}	ignition delay from SOC
θ	crank angle position [rad]
θ_{ig}	SOC crank position [rad]
t_d	injector delay
t_{d1}	time delay from ECU injector command to needle lift
t_{d2}	time delay from needle lift to actual start of injection
T	temperature in the cylinder
T_g	temperature of working fluid
T_W	wall temperature
U	internal energy
V	cylinder volume
V_c	clearance volume
V_d	displacement volume
$W_{c,I}$	indicated work per cycle

Subscripts

β	Watson shape parameter coefficient indicator for the proportionality factor
C_1	Coefficient indicator for Watson pre-mixed peak timing shape parameter
C_2	Coefficient indicator for Watson pre-mixed peak slope shape parameter
C_3	Coefficient indicator for Watson diffusion controlled burn rate shape parameter
C_4	Coefficient indicator for Watson diffusion controlled timing shape parameter
s	sensible

Chapter 1: Introduction

1.1 Overview and History of Diesel Engine

The diesel engine was developed by Rudolf Diesel in 1893 and utilizes the heat from high compression to ignite injected fuel in the cylinder. It has the highest thermal efficiency of any regular combustion engine, mainly due to its high compression ratio. Large, low speed diesel applications have seen thermal efficiencies over fifty percent [1]. The engine was originally used as a replacement for stationary steam engines. In the early 1900's, diesels were used in submarines, ships, locomotives, large trucks, and power generation. The first light duty on-road diesel applications were in the early 1970's. By 2007, about 50 percent of new car sales in Europe were diesel up from 10% in early 1990's [2]. Recent advancements in light duty on-road diesel engines include variable geometric turbochargers (VGT) for intake air control and operating efficiency, high pressure common rail fuel injection, and exhaust gas recirculation (EGR). All of these advancements are operated and controlled through the engine control unit (ECU) on a high speed CAN-bus network.

1.2 Motivation for Research

These advancements in engine technology cannot be operated without having an effect not only on the engine, but also the other accessory components. All the interactions between components in a diesel engine must be considered in order to maintain optimum performance and efficiency while minimizing emissions. The conventional approach has been to use dynamometer, or "off-board", testing to optimize

control parameters at a range of operating conditions, or to “map” the engine. This approach is extremely time consuming, considering the fast pace of new advancements in automotive technology. Computer upgrades, due to requirements for emissions regulations, have made it possible for “on-board” based computer control models. The primary goal of the project is to construct a diesel engine test stand that takes advantage of current diesel technology, including variable geometric turbochargers, multi-strike common rail fuel injection, EGR control, etc. Other automotive technology, such as drive-by-wire throttle, allows for easy integration of fuel load control into our data acquisition devices. Adaptability is also a major design criterion with the engine test stand. This setup will be used for future projects including emissions modeling and integration into hybrid vehicle applications. The features available in the current test stand can be seen in the diagram below:

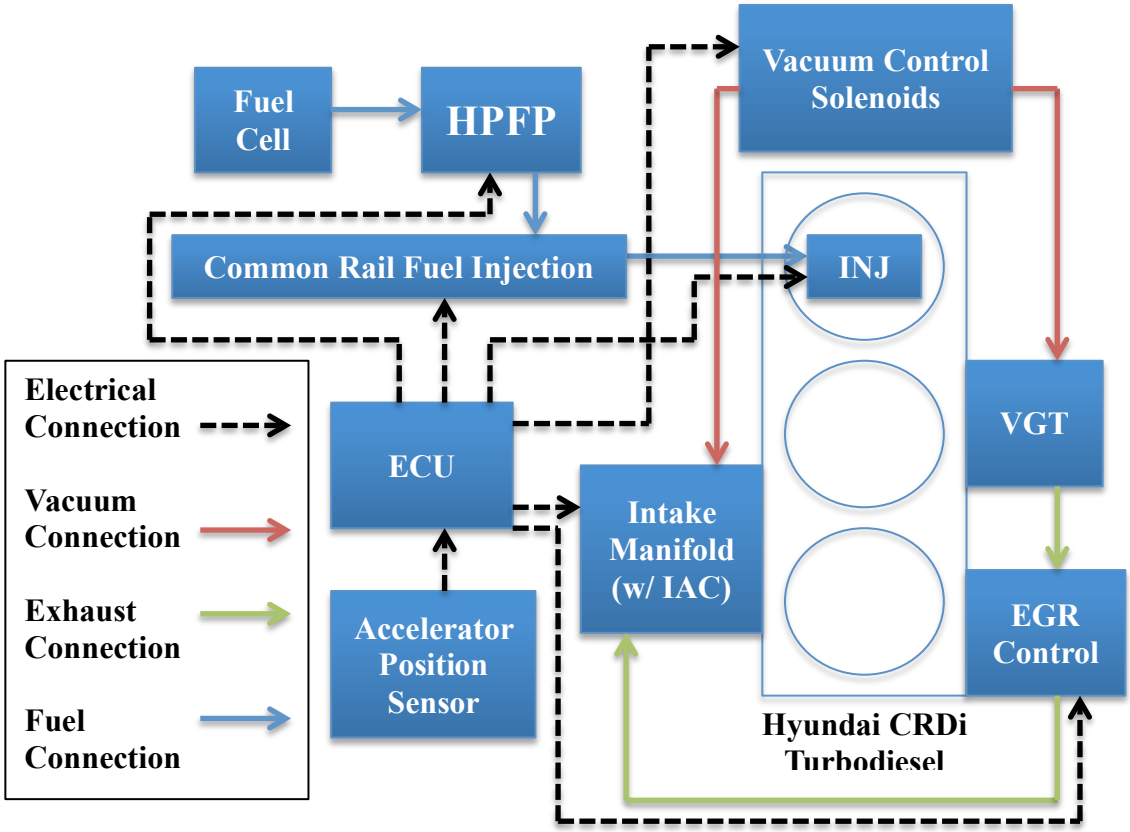

Figure 1 - 1: Diagram of Technology in Current Test Stand

The current test stand allows the user to input a specific engine fuel load and dynamometer brake load, thus controlling the engine speed. Once engine speed and brake load are set, the mean engine operating parameters, such as the operating temperatures, mass air flow (MAF) rate, intake manifold pressure (IMAP), and air/fuel ratio can be recorded. The test stand also has the ability to record crank angle based parameters, such as cylinder pressure, injector current, and fuel rail pressure.

The other goal of the research is to develop models in Matlab that can analyze the experimental pressure data to get quantitative information about the combustion process. These simulations use the principle of conservation of energy to determine the state of the working fluid and the amount of energy release during combustion. The simulation can

also calculate overall cycle values described in the section below. A sub-model is then created to estimate the energy release and burned fuel mass given specific inputs. This sub-model is calibrated using the energy release rate curves and can be substituted in the main simulation. The end result is an engine simulation that can predict the cylinder pressure and energy release rate. The importance of multiple fuel injections per cycle on the pressure traces and energy release curves will also be investigated.

1.3 Performance Standard Measurements

The cylinder pressure in an engine cycle is affected by combustion, the change in cylinder volume, and heat transfer with surrounding surfaces. The effect of the change in cylinder volume and combustion can be seen by comparing the motored pressure to the fired pressure. The pressure traces, energy release, and heat loss can be plotted based on the crank position. These plots make it possible to compare the effects and timing of compression, combustion, and expansion events over different dynamometer loads and engine speeds. A crank position vs. cylinder pressure plot for one of the test conditions can be seen in Figure 1-2.

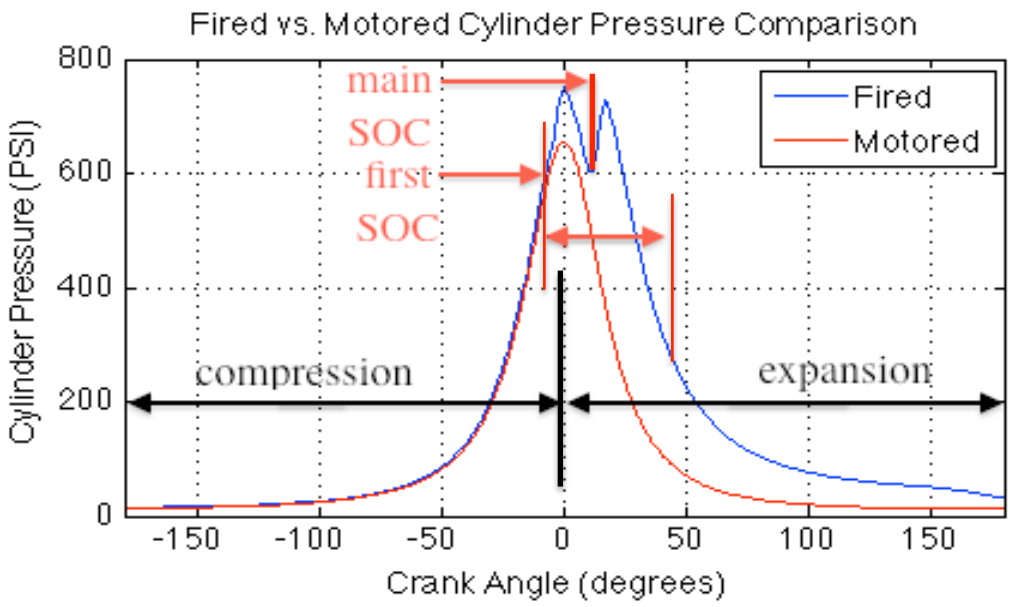

Figure 1 - 2: Location of Combustion Process Events

The effect of multiple fuel injections per cycle (FIPC) on the pressure trace can be seen in the plot above. Combustion begins at the first start of combustion (SOC) and continues to the end of the burning period for combustion of the main injection. The first SOC occurs at the separation of the fired pressure trace from the motored pressure trace. The main SOC and burning period can be located using the net heat release rate curves. Pressure-volume diagrams, also known as indicator diagrams, can be used to calculate the work transfer from the working fluid to the piston. An indicator diagram for one of the test conditions can be seen in Figure 1-3. A detailed explanation of generating P-V diagrams will be given later in the paper.

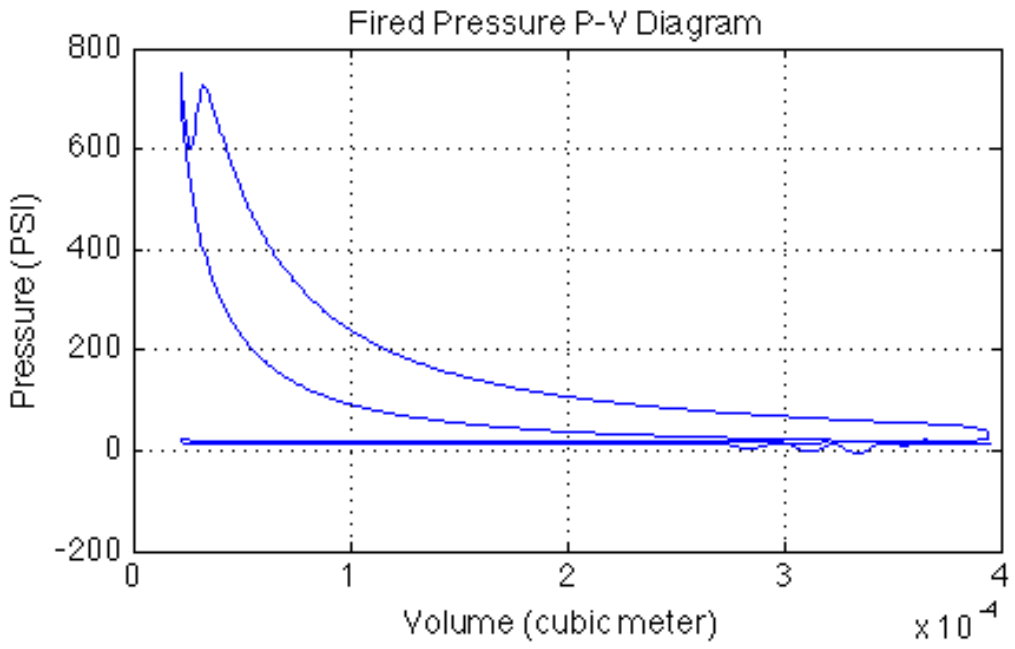

Figure 1 - 3: P-V Diagram of Fired Pressure Trace from Figure 1-2

Gas pressure acting on the piston surface does net work on the piston as the engine moves through its cycle. Overall engine operating characteristics are also calculated for comparison. The indicated work per cycle is obtained by integrating the compression and expansion curves in a P-V diagram

$$W_{c,i} = \int pdV \qquad (1.1)$$

Gross indicated work is the work delivered to the piston over compression and expansion strokes only. Net indicated work, or thermodynamic work, is the work delivered to the piston over the entire four-stroke cycle. Difference between thermodynamic work done on the piston and brake work measured at a dynamometer is the friction work [5]. Measured values of work are dependent on engine size. To provide a basis for comparing engines of different sizes, each of the above work terms can be divided by volume to get mean effective pressure. The mean effective pressure is the theoretical pressure at which constant pressure expansion from min to max cylinder volume would produce an amount

of work equal to the quantity being considered [3].

$$\text{IMEP [PSI]} = \frac{W_{c,i}}{V_d} \tag{1.2}$$

The specific fuel consumption using indicated power is calculated as

$$\text{ISFC} \left[\frac{\text{lbm}}{\text{hp} \cdot \text{h}}\right] = \frac{\dot{m}_f}{\dot{W}_{c,i}} \tag{1.3}$$

The indicated torque can be calculated using the IMEP value above:

$$\text{Torque} \left[\text{lb} \cdot \text{ft}\right] = \frac{\text{IMEP} \times V_d}{150.8} \tag{1.4}$$

The indicated torque can then be compared to the brake torque recorded by the dynamometer.

1.4 Structure of this Document

The following chapters explain the path taken in this research and the goals achieved as defined by the performance measurements. Chapter 2 gives a qualitative description of the combustion process in a diesel engine as well as defining the significance of the heat release rate to the combustion process. A brief overview of the range of combustion models and sub-models is also presented. Chapter 3 provides a detailed explanation of the single zone model, including the governing equations, heat release model, heat transfer model, and the fuel and trapped air models. Chapter 4 describes the diesel engine test stand, its individual components, and models. Chapter 5 involves the calibration of the heat release model with experimental test data. Chapter 6 describes the overall model with estimated heat release rate. Finally, conclusions are drawn along with recommendations for improving the test stand.

Chapter 2: Literature Review

2.1 Explanation of Combustion Process

The combustion process starts when fuel is injected into the cylinder near the end of the compression stroke, and it includes the ignition delay period, the rapid combustion phase, and the diffusion-controlled burning phase. Lyn completed the first explanation of the heat release in a diesel engine [3]. He observed many characteristics of the combustion process by reviewing injection rate and heat release diagrams. He summarized that the heat release rate for a single injection is formed by an ignition delay period, a premixed combustion phase, and a diffusion combustion phase. These phases form the total heat release rate in an engine, which is the rate of chemical energy release during combustion. The first stage of combustion involves the ignition delay and the rapid combustion phase. Ignition delay directly affects the processes and parameters in the heat-release period, including the pressure rise rate, maximum cylinder pressure, and IMEP. The rapid or premixed combustion phase is the result of the injected fuel mixing with air during the ignition delay and only lasts for a few crank angle degrees. The highest heat release rate is seen during this phase and is dependent on the amount of fuel-air mixture that is ready to burn. The second stage of combustion is the mixing-controlled phase, which is controlled by the rate that air and fuel mixes in the cylinder. The graphical representation of the total heat-release rate can be seen in Figure 2-1:

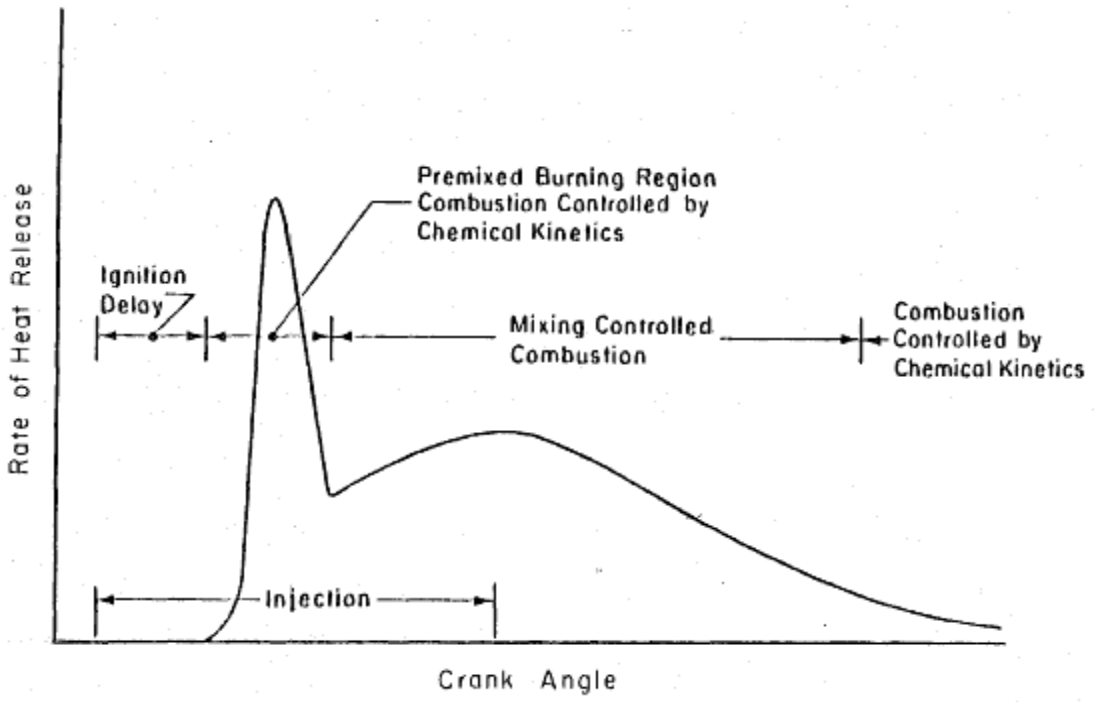

Figure 2 - 1: Engine Heat-Release Rate [3]

Ignition delay is defined as the time between the dynamic start of injection (SOI) and the start of combustion (SOC). The dynamic start of injection is defined as the start of the needle lift in the fuel injector. The start of combustion (SOC) is identified from the change in slope of the heat release rate, determined from cylinder pressure data. Multiple physical and chemical processes occur during the ignition delay period. The physical processes include the atomization of the fuel into droplets and the vaporization of the fuel droplets. Atomization is a function of fuel injection pressure, injector hole diameter, and cylinder pressure during injection. Vaporization is a function of the size, velocity, distribution, and ignition characteristics of the fuel droplets along with the conditions inside the cylinder, injection timing, and injection quantity. The chemical processes include the reactions that occur due to the fuel air mixing. Fuel-air mixing is a function of cylinder and piston design, along with nozzle arrangement of the injector [3]. Since the

premixed and diffusion-controlled phases of the heat-release rate are proportional to the ignition delay, it is critical to accurately define the ignition delay period.

2.2 Engine Models

Modeling gives a representation of a physical process through a combination of assumptions and equations. A sufficient engine model should include sub-models that represent the processes of engine subsystems, accurately predict the effect of key operating parameters over a wide range of loads and speeds, be adaptable with as little input from empirical data as possible, and have minimum execution time [4]. There are three main categories of engine models: linear, quasi-linear, and nonlinear. Linear models use transfer functions for relationships between inputs and outputs. These "black box" models are used to control operating parameters in real time applications, such as on an ECU, and do not include any in-cylinder thermodynamic calculations. Quasi-linear, or mean value, models are linear models based on physical sub-models, instead of mapping sampled data. These models can be used in real time with an upgraded computer. Two main types of nonlinear models exist for predicting engine performance and emissions on a crank-angle basis. The thermodynamic model is structured around energy conversion while the fluid dynamic model is based on fluid motion. Thermodynamic models are categorized as zero-dimensional, phenomenological, and quasi-dimensional (includes fuel spray behavior). Fluid dynamic models are also called multidimensional due to their ability to provide the geometry of the flow field. A summary of these models can be seen in Table 2-1.

	Linear	Quasi-Linear	Nonlinear	
			Thermodynamic	Multi-dimensional
Mathematical Complexity	Very Low	Low	High	Extremely High
Insight into the relevant phenomenon	Very Low	Low	Adequate	High
Program execution time	Negligible	Negligible	Limited	Very Large
Adaptability	Medium	Low	Medium-low	Medium

Table 2 - 1: Comparison of Engine Models [4]

One important fact to consider when choosing a model is to keep all parts of the model at the same level of sophistication. This will optimize efficiency since the accuracy of the model is dependent on its weakest link. A single-zone thermodynamic modeling approach is taken in this paper.

Single-zone models use the conservation of mass and energy to model the cylinder can be approximated as a control volume and the contents are at a uniform state. Their simplicity and low program execution time make them useful for approximating relatively complex diesel engine combustion process. These models use algebraic equations to match experimental heat release profiles [3]. A detailed explanation of the structure of the single zone model and sub-models is given in the next chapter.

2.2.1 Heat Release Models

The heat release rate, which is the rate of chemical energy release during combustion, can be estimated with algebraic equations. These estimations can be compared to heat release rates calculated from experimental pressure data. Many heat release rate estimation models have been proposed to quantify the phenomenological

observations made by Lyn. The goal of these estimations is to use the apparent fuel burning rate (AFBR) to predict the overall heat release to the cylinder. The Weibe function, popular in fuel mass burn rate predictions in spark ignition engines, has been applied in some models and can be seen below

$$M_b = \frac{m_b}{m_{f,inj}} = 1 - e^{\left[-C_A \left(\frac{\theta - \theta_{SOI}}{\Delta\theta_{duration}}\right)^{C_B}\right]} \quad (2.1)$$

Where: $M_b(\theta)$ is the burned gas fraction at a specified crank angle
θ_0 is the start of combustion (SOC),
$\Delta\theta$ is the burn period
C_A acts as a combustion efficiency coefficient and
C_B is a shape factor dependent on engine speed and equivalence ratio

The parameters in the Weibe curve are determined empirically based on experimental heat release curves. Since diesel combustion is divided into two distinct phases after SOC, a single Weibe function is a poor fit for diesel heat release analysis. Shipinski and Woschni [6] both used a double Weibe function to approximate the fuel burning mass, which provided a better fit than the single Weibe function. Watson developed an AFBR correlation that better matches the experimental heat release curves and one that could be used over a wider engine speed range compared to the Weibe function [7]. The Watson curve is specifically related to high speed direct injection diesel engines, and will be the correlation used in this model.

2.2.2 Heat Transfer Models

It is estimated that as much as one third of the fuel energy is passed on through heat transfer to the engine coolant and through the exhaust port. Heat transfer in the cylinder has an effect on overall engine performance, including engine efficiency and emissions. The heat transfer to the cylinder walls has a direct effect on the gas

temperature and pressure, which affects the work per cycle. While gas temperatures can reach over 3000ºF, the cylinder wall must be kept under 350ºF in order to prevent the breakdown of the oil film. Another consideration is the fatigue stresses on the engine block at high heat flux regions, which cannot exceed around 550ºF [3]. Heat transfer occurs by conduction, convection, and radiation. Conduction occurs through the cylinder head, walls, and through the piston. The bulk of heat transfer is forced convection between the in-cylinder gases and the cylinder head, cylinder walls, and the piston. Forced convection from the cylinder gases to the exhaust valves and port is also present during the exhaust stroke. Energy transfer by convection can be expressed as

$$\dot{Q}_{ht} = h_g A \Delta T = h_g A (T - T_W) \qquad (2.2)$$

Where: h_g is the convection heat transfer coefficient,
ΔT is the temperature difference between the gas and the cylinder wall,
A is the combustion chamber surface area

A general form for the convection heat transfer coefficient for multiple geometries is given by

$$\frac{h_g L_c}{k_c} = d Re^m Pr^n \qquad (2.3)$$

Where: Re is the Reynolds number
Pr is the Prandtl number
and d, m, and n are constants
k is the thermal conductivity
L is the characteristic length

A portion of the overall heat transfer in diesel engines is through the mode of radiation. The main sources of radiation are the soot particles formed in the flame and the high temperature gases. The hot surfaces in the cylinder, including the cylinder walls, piston, and gases in the cylinder, are approximated as black bodies. These black bodies emit or

absorb all radiation without reflecting any of it. The heat transfer from one black body at T_1 to another one at T_2 is given by

$$\dot{Q}_R = K_R A(T_1^4 - T_2^4) = \sigma C_R A(T_1^4 - T_2^4) \quad (2.4)$$

Where: σ is the Stefan-Boltzmann constant
K_R, C_R are calibration constants
A is the combustion chamber surface area

Approximating the in-cylinder gases as a black body is far from ideal, so a calibration constant is used. The significance of radiation in the heat transfer term is dependent on the particle size distribution, temperature, and number density [3]. These factors make it difficult to directly measure radiation in an operating engine. Also, the single zone combustion models use the mean cylinder temperature. This simplification can cause significant errors when the temperature is raised to the fourth power as in Eq. (2.4). Therefore, a majority of heat transfer models incorporate radiation effects in the heat transfer coefficient approximations given in Eq. (2.3).

The available engine models vary in accuracy, computational efficiency, and adaptability. The goal of the literary review is to find the best combination of sub-models to efficiently represent the combustion process while still maintaining a reasonable level of accuracy. The overall model must be highly adaptive to new sub-models that represent new technology or conditions.

Chapter 3: Modeling

3.1 Governing Equations

Cylinder pressure change is a function of the cylinder volume change rate, heat transfer, combustion, and mass flows into and out of the cylinder. Analyzing experimental cylinder pressure traces is a convenient method to determine the rate of heat release in an engine, especially when other contributing factors to cylinder pressure are known. The basis for any single-zone thermodynamic model is the application of the first law of thermodynamics to the cylinder. The model is quasi static (uniform temperature and pressure) and treats the cylinder as a control volume. The change in the internal energy of the system, U, is

$$\frac{dU}{dt} = \frac{dQ}{dt} - p\frac{dV}{dt} + \sum_j \dot{m}_j h_j \qquad (3.1)$$

Where: $\frac{dQ}{dt}$ is the heat-transfer rate through the system boundary

$p\frac{dV}{dt}$ is the work done by the system through the boundary displacement,

$\sum_j \dot{m}_j h_j$ is the energy due to mass flow across the system boundary.

In order to use a quasi-static open system, a few assumptions have to be made [3]:

1. Fuel injected into the cylinder is evaporated immediately so that fuel spray behavior will have no effect on the model. In reality, liquid fuel evaporates and mixes with air to produce a non-uniform fuel/air distribution.
2. The working fluid is a homogeneous ideal gas mixture

3. Crevice flow, including the charge trapped in the volume between piston, rings, and cylinder, is considered to be negligible. In reality, the crevice volume constitutes a few percent of the clearance volume and reduces the actual cylinder pressure.
4. Combustion is modeled as a uniformly distributed heat release, which is assumed to be proportional to the AFBR based on the above assumptions.

The assumptions above limit the mass flow across the boundary to be only the fuel injected. The accuracy of representing the processes in the cylinder with an energy balance equation depends on how the individual terms are defined. Eq. (3.1) is modified to pertain only to sensible energy in order to solve for the apparent heat release rate (AHRR). The heat release terms are labeled apparent since this method is an approximation of the real heat release quantities in the combustion process, which cannot be determined directly. The net heat release rate, $\frac{dQ_n}{dt}$, becomes the difference between the gross heat release rate, $\frac{dQ_{ch}}{dt}$, and the heat transfer rate to the surrounding environment, $\frac{dQ_{ht}}{dt}$. The sensible enthalpy of the injected fuel can be approximated as zero, so Eq. (3.1) becomes

$$\frac{dU_s}{dt} = \frac{dQ_n}{dt} - p\frac{dV}{dt} = \frac{dQ_{ch}}{dt} - \frac{dQ_{ht}}{dt} - p\frac{dV}{dt} \qquad (3.2)$$

Since the working fluid is an ideal gas, the left side of Eq. (3.2) can be represented as a function of the mean charge temperature only:

$$\frac{dU_s}{dt} = \frac{d(mu(T))}{dt} = mc_v\frac{dT}{dt} + u\frac{dm}{dt} \qquad (3.3)$$

Crevice effects represent the majority of mass flows into and out of the system. Since one of the assumptions above is to ignore crevice effects, the mass rate term in Eq. (3.3) can be ignored. Since the heat release model is based on experimental pressure traces, the temperature rate term needs to be substituted with pressure. Differentiating the ideal gas equation will yield:

$$\frac{\dot{P}}{P}+\frac{\dot{V}}{V}=\frac{\dot{m}}{m}+\frac{\dot{T}}{T}\ \rightarrow\ \dot{T}=T(\frac{\dot{P}}{P}+\frac{\dot{V}}{V}-\frac{\dot{m}}{m}) \tag{3.4}$$

Substituting the results from Eqs (3.3) and (3.4) into Eq. (3.2) yields

$$\frac{dQ_n}{dt}=\left(1+\frac{c_v}{R}\right)p\frac{dV}{dt}+\left(\frac{c_v}{R}\right)V\frac{dP}{dt} \tag{3.5}$$

Eqs. (3.4) and (3.5) are combined in order to easily relate the heat release model describe in the next section. This equation is converted to a crank angle basis using the relationship $\frac{d}{dt}=w\frac{d}{d\theta}$, where ω is the angular velocity of the engine . The equation can also be arranged to solve for the differential pressure.

$$\frac{dQ_{ch}}{d\theta}-\frac{dQ_{ht}}{d\theta}=\left(\frac{\gamma}{\gamma-1}\right)p\frac{dV}{d\theta}+\left(\frac{1}{\gamma-1}\right)V\frac{dP}{d\theta} \tag{3.6a}$$

$$\frac{dP}{d\theta}=\left(\frac{\gamma-1}{V}\right)\frac{dQ_{ch}}{d\theta}-\frac{dQ_{ht}}{d\theta}-\left(\frac{\gamma}{V}\right)p\frac{dV}{d\theta} \tag{3.6b}$$

3.2 Heat Release Model

The relationship between the AFBR and the AHRR is linearly proportional as long as the equivalence ratio of the mixture is less than one and there are no dissociation effects. The relationship is based on the assumption of a constant thermodynamic and chemical equilibrium, and the assumption that all of the fuel injected burns despite of the equivalence ratio [3]. The relationship between the AFBR and the AHRR can be

expressed as:

$$\frac{dQ_{ch}}{d\theta} = Q_{LHV}\frac{m_b}{d\theta} \tag{3.7}$$

Where: The lower heating value for diesel fuel, $Q_{LHV} \approx 42.612 \times 10^{-03}$ J/g
$\frac{dQ_{ch}}{d\theta}$ is the apparent heat release rate used in Eq. (3.5)

The combustion process is considered to begin at the point of injection and consists of an ignition delay period followed by a heat release period.

3.2.1 Watson Combustion Model

Watson developed a heat release rate correlation based on the phenomenological description of combustion discussed in chapter 2 [7]. An AFBR correlation is used to estimate the heat release rate by using Eqs (3.5), (3.6), and (3.7). The goal of Watson's correlation is to obtain an accurate and reliable correlation of the rate of heat release with engine operating parameters. The AFBR is represented by the two main phases of heat release: the premixed phase and the diffusion-controlled phase.

$$\frac{dm_b}{d\theta} = \frac{dm_p}{d\theta} + \frac{dm_d}{d\theta} \tag{3.8}$$

Watson weighs Eq. (3.8) with a proportionality factor, β, and non-dimensionalizes the independent variable, the crank-angle position.

$$\frac{m_b}{m_{f,inj}} = \beta f_1 + (1-\beta) f_2 \tag{3.9a}$$

$$f_1 = 1-(1-\tau^{C_1})^{C_2} \tag{3.9b}$$

$$f_2 = 1 - e^{(-C_3\tau^{C_4})} \tag{3.9c}$$

Where: C_1, C_2, C_3, C_4, and β are all empirically determined shape parameters
$\tau = \frac{\theta-\theta_{ig}}{\Delta\theta_b}$ is the dimensionless time from SOC
$\Delta\theta_b = \theta_{end} - \theta_{ig}$ is a user-defined burn duration period

3.2.2 Watson Shape Parameters

Eq. (3.9) represents the AFBR as a sum of two dimensionless burning modes weighted by a proportionality factor. The proportionality factor determines the significance of each mode of heat release on the total AFBR. The expression for the proportionality factor is the fuel burnt in the premixed phase as a fraction of the total fuel injected. This factor is a function of the ignition delay and the equivalence ratio as can be seen below

$$\beta = \frac{m_b}{m_{f,inj}} = 1 - \frac{0.95\varphi_{ig}^{\,0.41}}{\tau_{id}^{\,0.28}} \tag{3.10}$$

Where: τ_{id} is the ignition delay [ms]
φ_{ig} is the trapped equivalence ratio

The shape factors C_1 and C_2 are used to control the shape of the pre-mixed fuel burn rate. C_1 controls the timing of the peak while C_2 controls the slope of the rise and fall characteristic of the peak. C_1 is dependent upon the ignition delay and the engine speed. Watson's equation for predicting C_1 can be seen below

$$C_1 = 1.25\times10^{-8}(\tau_{id}N)^{2.4} \tag{3.11}$$

Where: τ_{id} is the ignition delay [ms]
N is the engine speed [RPM]

Watson's experimental results showed that the shape of the peak improved with high values of C_2 up to 5000 with marginal benefits deviating from this point. The shape factors C_3 and C_4 influence the diffusion-controlled mode of the heat release. C_3 changes the rate of diffusion and, ultimately, the burn duration. The shape factor is dependent upon the equivalence ratio, as can be seen in Watson's equation:

$$C_3 = \frac{14.2}{\varphi_{ig}^{0.644}} \tag{3.12}$$

Where: φ_{ig} is the trapped equivalence ratio

C_4 has a main influence on the timing of the peak burning diffusion rate. Watson notes the strong interaction between C_3 and C_4 as can be seen in the equation for C_4 :

$$C_4 = 0.79 C_3^{0.25} \tag{3.13}$$

3.3 Heat Transfer Model

A relationship proposed by Woschni has been proven to give reliable results in four stroke direct-injection engines [8]. The heat loss rate term is expressed as

$$\frac{dQ_{ht}}{dt} = Ah_g(T_g - T_w) \tag{3.14}$$

The heat transfer coefficient, h_g, in Eq. (3.14) can be calculated by

$$\begin{aligned} h_g\left(\frac{W}{m^2K}\right) &= C(\rho\upsilon)^b L^{(b-1)} T^{(0.76-1.62b)} \\ &= C(\rho(\upsilon_m + \upsilon_{comb})^b L^{(b-1)} T^{(0.76-1.62b)} \end{aligned} \tag{3.15}$$

Where: C,b are constants
υ is the characteristic speed
L is the characteristic length

Woschni set the constants b =0.8 and C=3.26, which applies for turbulent flow in pipes. The cylinder bore diameter is then set as the characteristic length. The characteristic speed depends on two terms. The first term is due to piston motion and can be modeled as

$$\nu_{mot} = C_{mot}\nu_{pis} \tag{3.16}$$

Where: ν_{pis} is the mean piston speed [m/s] and
C_{mot} is a constant dependent upon the particular process of the cycle

The other term is due to swirl in the combustion event and it is a function of pressure rise during combustion.

$$\upsilon_{comb} = C_{comb} \frac{V_d \, T_{ref}}{p_{ref} V_{ref}} (p - p_{mot}) \qquad (3.17)$$

Where: T_{ref}, V_{ref}, p_{ref} are taken at an arbitrary reference point (IVO or SOC)
C_{comb} is another constant dependent upon the particular process of the cycle
p_{mot} is the measured motor pressure

The constants C_{mot} and C_{comb} in Eqs (3.16) and (3.17) are defined for each process of the combustion cycle:

For the gas exchange period: $C_{mot} = 6.18$ $C_{comb} = 0$

For the compression period: $C_{mot} = 2.28$ $C_{comb} = 0$

For the combustion and expansion period: $C_{mot} = 2.28$ $C_{comb} = 3.24 \times 10^{-3}$

3.4 Engine Geometry

The cylinder volume at any crank position can be calculated using the following equation

$$\frac{V}{V_c} = 1 + \frac{1}{2}(r_c - 1)[R_v + 1 - \cos(\theta) - (R_v^2 - \sin^2\theta)^{1/2} \qquad (3.18)$$

Where: V_c is the clearance volume [m^3]
r_c is the compression ratio
$R_v = \frac{2l}{s}$ is the ratio of connecting rod length (l) to stroke (s)
θ is the crank position [rad]

Eq. (3.19) can be differentiated to give the term $\frac{dV}{d\theta}$ needed in the governing equations. The combustion chamber surface area at any crank position θ is

$$A = A_{ch} + A_P + \frac{4V}{B} \qquad (3.19)$$

Where: A_{ch} is the cylinder head surface area
B is the bore
$A_p = \pi \frac{B^2}{4}$

The combustion chamber surface area is needed to calculate the heat transfer rate in Equation (3.14).

3.5 Fuel Injection Model

The fuel is introduced into the cylinder at a large pressure differential across the nozzle orifice. The cylinder pressure at injection is in the range of 750 to 1500 psi. Fuel injection ranges from 4000 to 20000 psi. The large pressure difference is required so that the injected liquid fuel jet will enter the chamber at sufficiently high velocity to (1) atomize into small droplets for rapid evaporation and (2) spread through the entire combustion chamber in the time available to fully utilize the air charge. In an electronic injector, a solenoid operated control valve is used to control the fuel input. The injection timing and duration is controlled by the ECU. Assuming flow through each nozzle is quasi steady, incompressible, and one dimensional, the mass flow rate of the fuel injected through the nozzle is given by the following equations from Assanis [9]:

$$\dot{m}_f \left[\frac{g}{s}\right] = C_D A_n \sqrt{2\rho_f \Delta P} \tag{3.20}$$

Where: C_D is the discharge coefficient
A_n is the nozzle minimum area [m^2]
ΔP is the pressure drop across the nozzle [Pa]
ρ_f is the fuel density [g/m^3]

The mass of the fuel injected can then be determined by

$$m_f\,[g] = C_D A_n \sqrt{2\rho_f \Delta P} \frac{\Delta\theta}{6N} = C_D A_n \sum_{SOI}^{EOI} (2\rho_f \Delta P)^{1/2} d\theta \tag{3.21}$$

Where: N is the engine speed [RPM]
$\Delta\theta$ is the duration of the fuel injection [rad]

During steady-state testing, standard flowmeters can be used to measure fuel and air flow rates. The air/fuel (A/F) ratio can also be measured using the same technique with a wideband O_2 sensor. However, these sensors do not have the ability to measure on a cycle-by-cycle basis. An entire engine cycle at idle (890 RPM) lasts 0.135 seconds and 0.06 seconds at 2000 RPM. We do not have the ability to directly measure the mass of fuel injected and the amount of air trapped for each cycle. In order to determine the injector discharge coefficient, C_D, the engine is operated at steady state conditions. The mass of fuel injected per cycle, as given in Eq. (3.21), is computed from fuel flow rate measurements. The fuel flow rate can be determined directly from the change in weight or from the MAF and A/F ratio. The integral, which appears on the right hand side of Eq. (3.21), can be computed using values for the instantaneous pressure difference between the fuel injection pressure and the cylinder pressure between SOI and EOI.

Start of Injection (SOI) is signaled by an ECU command, which can be measured directly as a current signal and pulse width (PW). For a given fuel injection command, there will be a delay from the command to the needle lift and then a second delay between the needle lift and the start of actual fuel injection. The total delay is the sum of the individual delays. These time delays are calculated to determine the crank angle position of actual fuel injection. Since a needle lift sensor has not been installed in this test stand, the delay from the ECU command to the injector needle lift is estimated from an empirically based equation developed by Gong [10]. The first delay time is related to the magnetic and hydraulic force exerted on the injector plunger. Therefore it is not a function of injection pressure or pulse width. The second delay time is the time between

the needle lift and the point of actual fuel injecting into the chamber. This time includes the transport delay for fuel flow and can be assumed to be 0.1 milliseconds.

$$t_d = t_{d1} + t_{d1} \tag{3.22a}$$

$$t_{d1}[\text{ms}] = 0.4815 - 0.0001313P_r - 0.00024P \tag{3.22b}$$

Where: P_r is the fuel rail pressure [bar]
P is the cylinder pressure [bar]

3.6 Trapped Air Model

The trapped air mass during the intake stroke will be estimated using the average MAF rate. The trapped air mass can be calculated by

$$m_a\,[\text{g}] = 453.59 \times \frac{d\bar{m}_a}{dt} \frac{1}{N} \frac{\text{Revolutions}}{\text{Intake Strokes}} \tag{3.23}$$

Where: N is the engine speed [RPM]
$\frac{d\bar{m}_a}{dt}$ is the average MAF rate from experimental data [lb/min]

3.7 Supporting Models

Models developed by Olikara and Borman [11] are used to predict the unburned and burned gas mixture at different stages of the engine cycle. These models take into account the changing composition of the working fluid and accurately predict state properties such as specific enthalpy, internal energy, entropy, gas constant, and specific heats. The program uses fitted JANAF polynomial curves divided into two temperature ranges: below 1000K and between 1000K and 5000K. These programs were modified by Buttsworth [12] to use in Matlab. Minor changes have been made to these programs in order to incorporate them into the main combustion model, but the changes do not affect the overall output of the programs.

3.8 Model Diagram

A model diagram, shown in Figure 3-1, has been created to show how the different sub-models interact. An initial condition is defined at crank angle $\theta = -180°$. This initial condition includes an initial pressure and temperature. The process is controlled by crank position and new values are calculated every increment (0.36°). The dashed line represents crank angle position. The output values are used as inputs to the sub-models and initial guesses for the governing differential equations in the next iteration. First, the model defines the engine constants for the entire cycle including cylinder geometry, fuel and injection properties, initial operating conditions, combustion model properties, injected fuel mass, and trapped air mass. The next step is to calculate the heat release and heat loss rates, along with the equilibrium properties, for the current iteration. These values are used as inputs to the governing equations. The procedure is then repeated for the entire crank period, from $\theta = -180°$ to $\theta = 180°$.

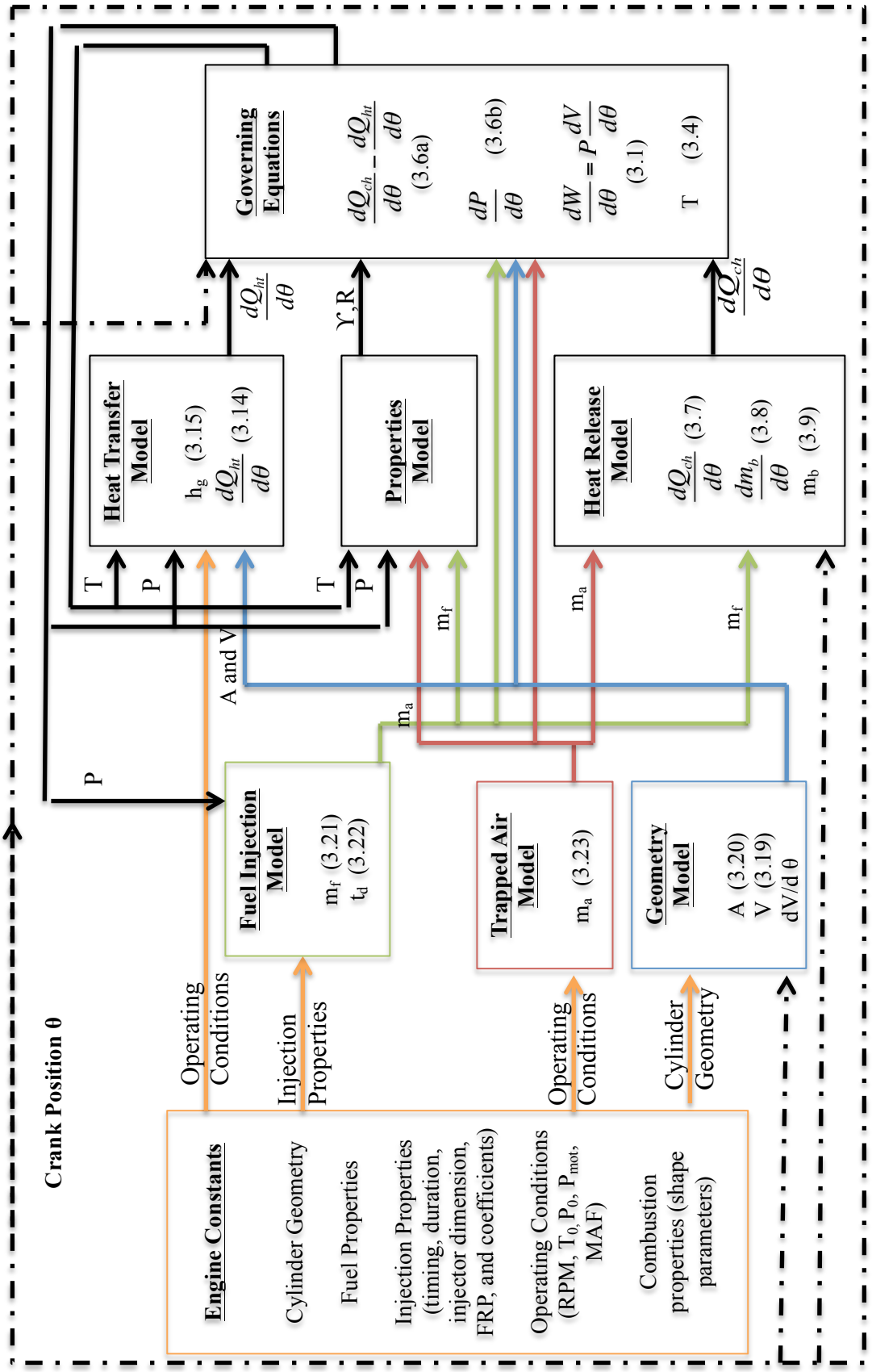

Figure 3 - 1: Diagram of Combustion Model

Chapter 4: Experimental Setup

4.1 Introduction

This chapter describes the components of the test stand, along with the user-written control and monitoring programs in LabVIEW. A detailed explanation of the calibration process for the in-cylinder pressure sensor and the filtering of the raw pressure data is also included.

4.2 Diesel Engine Test Stand and Dynamometer

The test stand uses a 1.1L three cylinder turbocharged diesel engine from Hyundai/Kia of South Korea. The engine load is applied by a 13" toroidal dynamometer and controlled by a servo-operated load valve. The basic engine specifications can be seen in Table 4-1. The coolant system features a shell and tube heat exchanger, with water entering the shell through a 2" main at 45 psi and exiting to a dump pipe. Hot coolant enters the tube inlet and exits to the water pump. The fuel system uses a five gallon racing fuel tank and delivers fuel by gravity feed to the fuel filter and then the engine. The major components of the test stand were already in place, but considerable work was put into retrofitting it for cycle-by-cycle analysis.

Manufacturer	KIA/HYUNDAI
Type	I-3 DOHC
Displacement	1120 cc
Bore x Stroke	75.00mm x 84.50 mm

Compression Ratio	17.80:1
Fuel System	Common Rail Direct Injection
Aspiration	Turbocharged
Max. Output	74.0 bhp at 4000 RPM
Max Torque	113 lb-ft at 1900 RPM
Redline	4500 RPM
Idle	890 ± 100 RPM

Table 4 - 1**:** Hyundai Engine Specifications

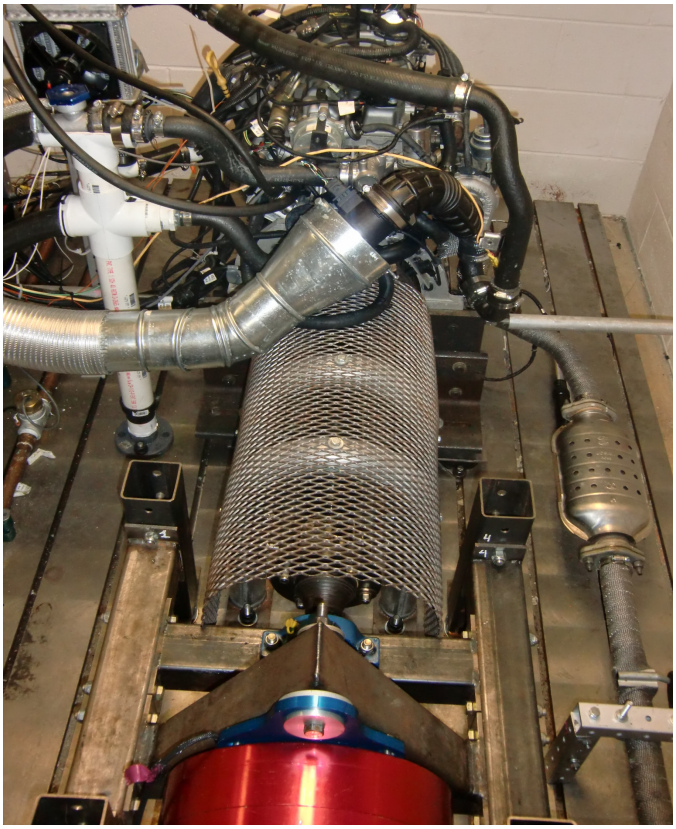

Figure 4 - 1: Engine Test Stand and Dynamometer

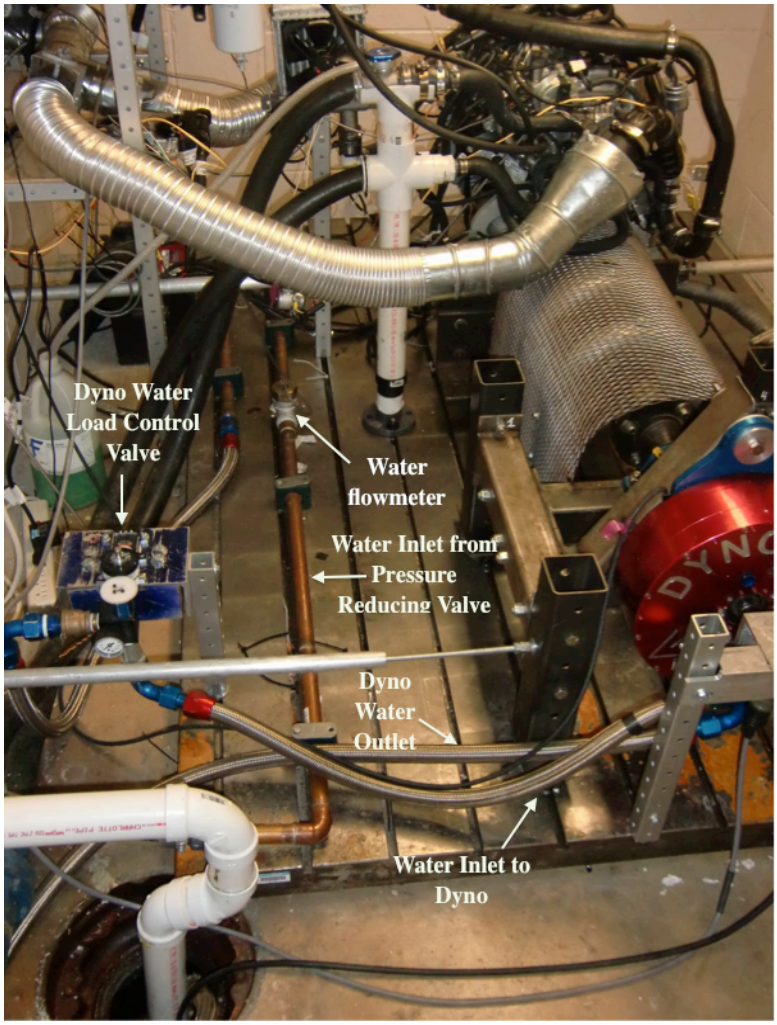

Figure 4 - 2: Dynamometer water flow configuration

The dynamometer is a 13" single-stator absorber from Land and Sea that operates at 10 PSI dynamic pressure and 30 PSI static pressure for testing purposes. The water flows through a pressure reducing valve from the 2" city main to regulate the pressure between 10-35 psi. A paddle wheel flow sensor is installed between the pressure regulator and the servo load valve to measure water flow going to the dynamometer. A servo motor is used to control the position of the position of the load valve for the dynamometer.

4.3 Sensors

Two different groups of sensors are used to obtain all the necessary information about the operating condition of the engine. The following sensors are used to measure the mean operating parameters of the engine and are on a relatively slow time base (sampling 2 to 10 Hz).

Temperature: Intake (at Filter) Intake (at manifold) Oil (at crankcase) Coolant (pump outlet) Exhaust (downpipe) Dyno Outlet	Omega K type thermocouples National Instruments TC01 conditioning modules
Intake Manifold Pressure	Calibrated Voltage input from OEM Sensor
Load Torque	full bridge strain gauge (Land and Sea) National Instruments SG-04 conditioning module
Mass Air Flow	Calibrated Voltage input (counter) from OEM sensor
Air/Fuel Ratio	Innovate Motorsports LC-1 lambda sensor
Dyno Flow	Omega FP7001A paddlewheel flow sensor
Engine Speed	BEI H25D Incremental Encoder

Table 4 - 2: List of Mean Operating Sensors

The fuel cell is placed on a SVI-20B digital scale. This scale has a RS-232 input and a measurement is taken every two seconds to determine the overall fuel consumption. The other group of sensors is used to measure operating parameters on a crank angle basis. The sampling rate is very high at 50,000 to 150,000 Hz.

In-cylinder Pressure	Kistler 6056A Kistler 5010B charge amplifier
Injector Current	Tektronix A6302 current probe Tektronix TM502A charge amplifier
Fuel Rail Pressure	Calibrated Voltage input from OEM Sensor
Crank Angle Position	BEI H25D Incremental Encoder

Table 4 - 3: List of High Speed Sensors used in Engine Test Stand

Figure 4 - 3: Kistler 5010b Charge Amplifier

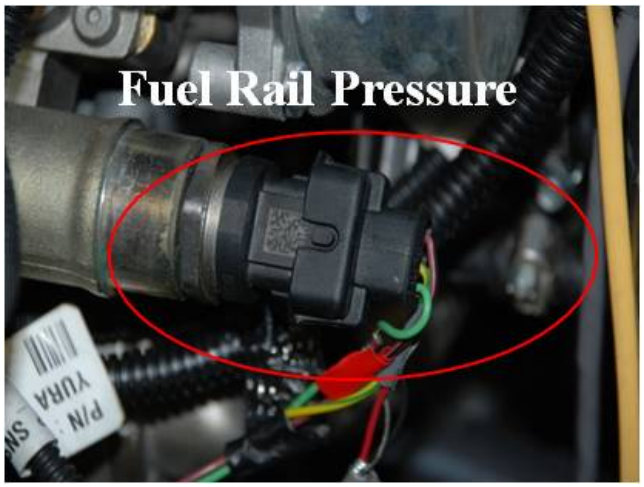

Figure 4 - 4: Fuel Rail Pressure Sensor Location

Figure 4 - 5: Kistler Pressure Sensor and Glow Plug Adapter

Figure 4 - 6: Tektronix Current Probe attached to Cylinder 1 Injector wire

4.4 LabVIEW programs

The easiest method to relate cylinder pressure and various combustion-related events is to reference them to the crankshaft position. A BEI H25D incremental encoder is used to measure crank angle position. The encoder has a resolution of 1000 cycles per revolution and it is mounted to the splined shaft of the dynamometer. A

National Instruments PCI-6259 Data Acquisition card, along with a National Instruments SCB-68 breakout board, is used to input the measured signals from the second group of sensors into the computer. Measured signals are scanned at a constant rate from the DAQ card. This scan rate is defined in a user written labVIEW program. The PCI-6259 is a 16-bit Multichannel DAQ card capable of 1.25 mega-samples per second [MS/s]. The program samples data off of the card at each pulse of the incremental encoder to capture cylinder pressure, injector current, and fuel rail pressure data points. The Sampling Theorem calls for the scan rate to be adjusted to be at least twice the encoder rate in order to avoid aliasing in the data [13]. Figure 4-7 shows the front panel of the crank-angle based LabVIEW recording program.

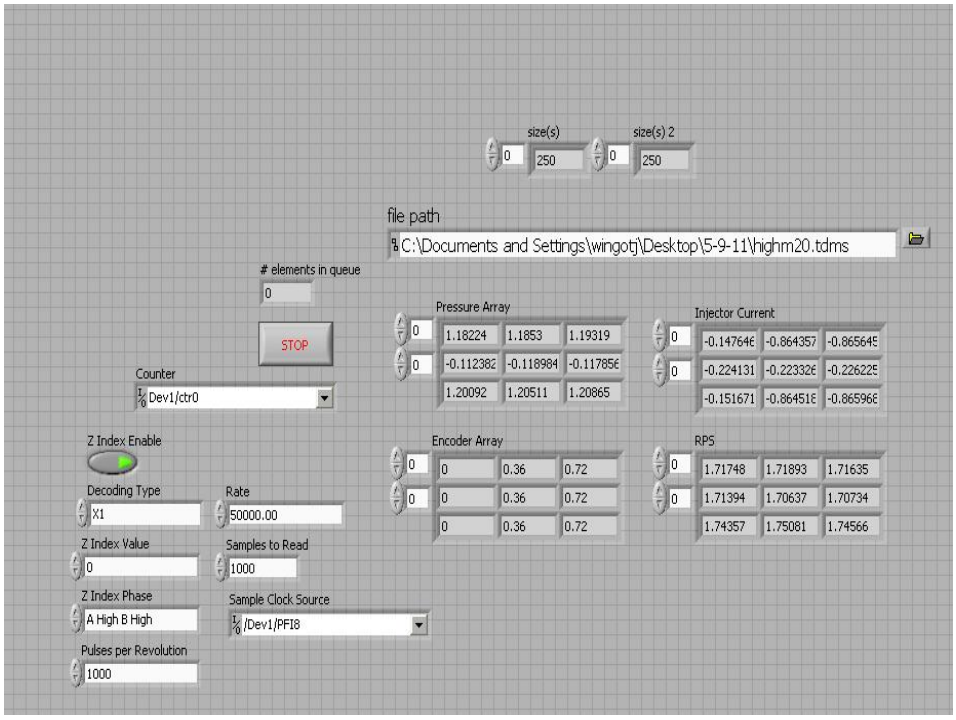

Figure 4 - 7: LabVIEW High Speed Program

Figure 4 - 8: SCB-68 breakout board for crank angle based inputs

The data is placed into individual arrays for the cylinder pressure, injector current, fuel rail pressure, and encoder position. These arrays are then saved as sheets in Excel. A separate LabVIEW program is used for engine fuel and dynamometer load control. A NI PCI-6025E DAQ card and SCB-68 breakout board are used to output the signals to the ECU and servo motor on the load valve. The engine fuel control sends a variable voltage signal to the accelerator position sensor. The dynamometer load control is a pulse width modulation (PWM) signal that determines the position of the servo motor on the load valve. Water flow into the dynamometer is measured by a paddlewheel flow sensor. The frequency of the signal is measured through a counter input and converted to gallons per minute (GPM). Figure 4-10 shows the front panel of the fuel and dynamometer load control program.

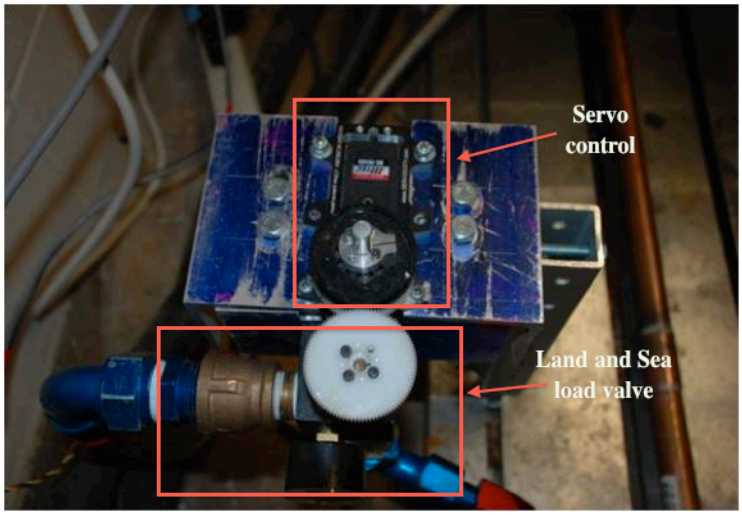

Figure 4 - 9: Servo Load valve control

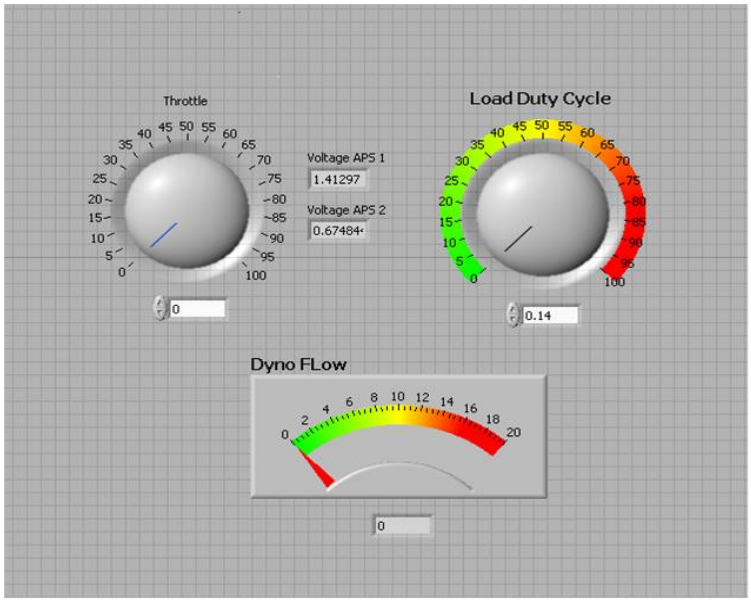

Figure 4 - 10: LabVIEW Engine Control Program

4.5 Detailed Explanation of Crank Angle Encoder

Accurate crank angle position and volume measurements are critical to obtain reliable pressure traces. A picture of the encoder setup can be seen in Figures 4-11 and 4-12.

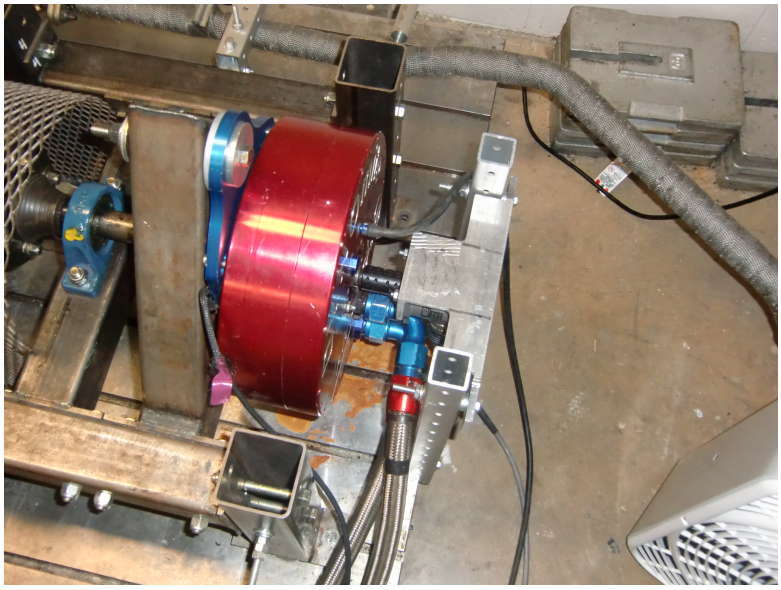

Figure 4 - 11: Encoder mount to dynamometer

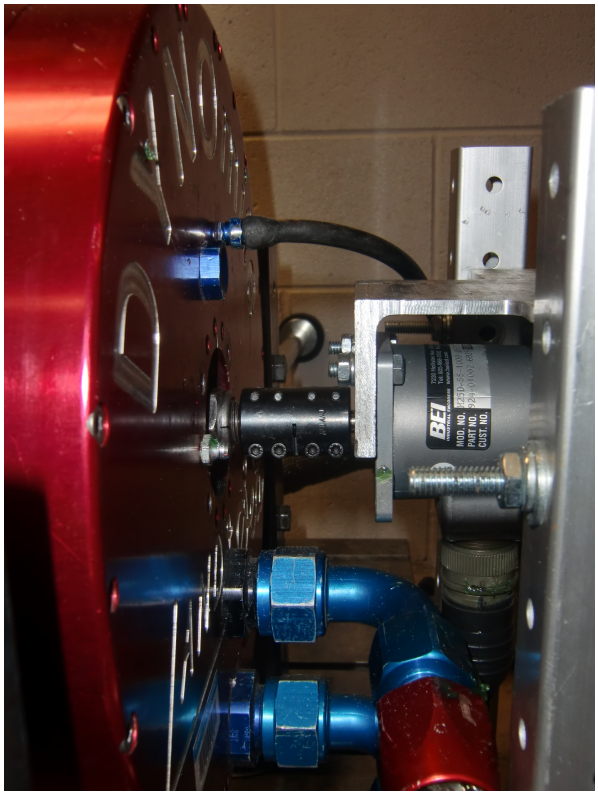

Figure 4 - 12: Zoom view of encoder mount

The total cylinder volume at any given crank angle position is the sum of the clearance volume and the volume due to piston motion. The volume due to piston motion is based on cylinder geometry already discussed in Chapter 3. Since the cylinder dimensions are known, the accuracy of the total cylinder volume depends on the clearance volume measurement and the crank angle position [14]. The timing of many of the cycle processes is related to TDC, so it is convenient to know the exact encoder position relative to TDC. Also, the phasing of pressure data has proven to be the most significant in terms of the change in pressure, heat release and burned mass. A dial indicator is used to record the piston displacement versus encoder position. A best-fit line is applied to the data to determine the exact crank angle position of TDC. Once TDC is found, the encoder is reset so zero degrees crank angle (CA) will correspond to TDC. A picture of the test setup and of the test data can be seen in Figures 4-13 and 4-14.

Figure 4 - 13: TDC test setup

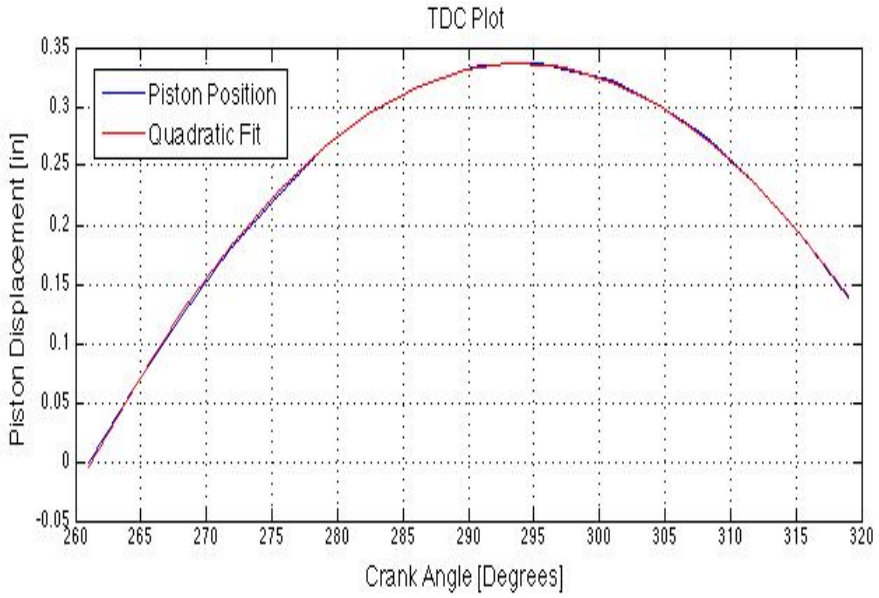

Figure 4 - 14: Graph of Measured Piston Travel and Best-Fit Approximation

4.6 Detailed Explanation of Piezoelectric Pressure Sensor

The cylinder pressure measurement system consists of a Kistler 6056A piezoelectric pressure transducer and a Kistler 5010b dual mode charge amplifier. The pressure transducer produces a charge that is related to a relative pressure change in the cylinder. The transducer uses quartz as the sensing element due to its high stress limit, good temperature resistance, high rigidity, and high linearity. The charge amplifier is comprised of a high gain inverting voltage amplifier with a MOSFET input for high insulation resistance. The purpose of the charge amplifier is to convert the charge signal from the transducer into a high-level voltage output that can be read by a DAQ system [15]. The Kistler 6056A sensor is a dry sensor, so it is susceptible to thermal shock. Thermal shock is the error in the signal due to the deformation of the transducer from hot combustion gases. This error is most prominent near the end of expansion and exhaust cycle processes, and it is known as the “bowtie” effect. Despite the fact that this sensor is

specifically designed and calibrated to operate within a given temperature range, thermal shock can never be completely removed [14]. The pressure transducer is mounted in an adapter piece that fits in the OEM glow plug position, as shown in Figure 4-15.

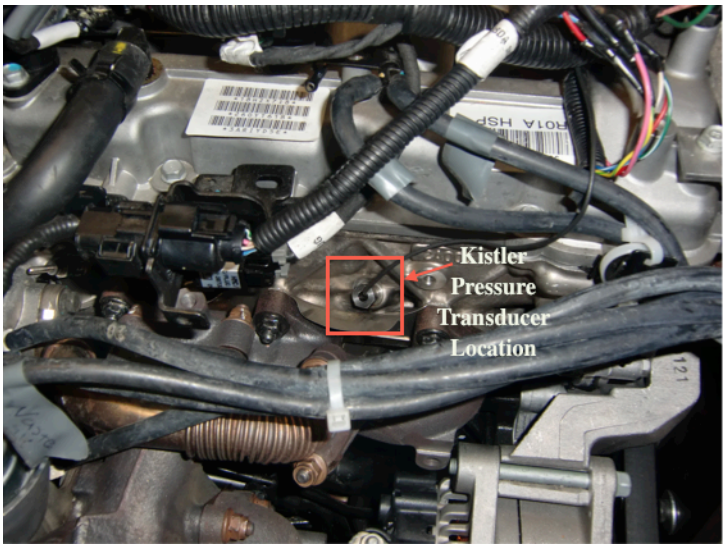

Figure 4 - 15: Pressure transducer installation

4.6.1 Charge Amplifier Calibration

The processing of electrical charges requires high insulation resistance in the system. Typical resistance values are on the order of 10^{13} Ohms. Despite the high resistance, charge leakage does occur. Charge leakage, or drift, is an erroneous change in transducer output over time that is not related to the measured signal. The time constant is the time it takes for the charge signal to decay, or charge leakage rate. This decay can cause low readings during expansion and can cause errors during the compression phase. The best way to minimize decay is to increase the time constant until signal drift is encountered [14]. The charge amplifier has an effect on the charge leakage, and subsequently the accuracy of the measured pressure. Drift can be caused by low insulation resistance in the connections and the input or by leakage current at the

MOSFET. The time constant of the transducer system is a measure of the time it takes for the signal to decay and not a measure of the input response of the system. Drift and the time constant have a simultaneous effect on the output in which one or the other will dominate [15]. The connections of the system must also be kept clean and condensation free in order to prevent signal drift.

4.6.2 Screening Raw Pressure Data

For each test condition, one hundred consecutive cycles are recorded and then averaged. Averaging consecutive cycles of pressure traces is the recommended practice to obtain reliable data for two reasons. The first reason is that averaging the pressure traces fixes any abnormal variances that might be seen during individual pressure traces. Also, air and fuel mass flow rates are recorded as averages of steady-state values. Therefore, an average of experimental pressure traces will have a better correlation with the averages of the fuel and air mass flows. The number of cycles to record is based on the variability of each cycle. The goal is to record enough cycles to fully capture the cyclic variability of the data, but to not record so long that the operating speed and load change appreciably. We had some issues maintaining a constant water supply pressure during initial testing. Before the average pressure data can be used, it must be scaled. The charge amplifier gain and sensitivity are used to convert the charge signal into the preferred measuring unit (PSI, bar, etc.). These settings can be modified on the amplifier and affect the voltage output from the amplifier to the DAQ system. The output from the charge amplifier does not give a DC offset, since the pressure signal is AC coupled. The relative pressures are shifted to an absolute pressure value at a known crank angle position to obtain absolute cylinder pressure. This procedure is known as pegging [14].

Accurate cylinder pressure pegging is needed to find not only the peak cylinder pressure and polytropic coefficients, but also to calculate the heat release rates. In this model, the relative pressure at BDC after the intake stroke is assigned the absolute pressure value in the intake manifold at that instant in the cycle.

4.6.3 Verifying Motored Runs

Motored pressure traces are not affected by combustion-related complications and inhomogeneities. These traits make motored pressure traces ideal for checking the calibration of the pressure sensor. The first check is the phasing of pressure with respect to volume near TDC. In theory, the peak pressure should occur slightly before TDC due to irreversibilities caused by heat transfer. If the peak pressure occurs at or later than TDC, the pressure data is retarded with respect to volume. On the other hand, if peak pressure occurs more than two degrees before TDC, the pressure data is advanced. As can be seen in Figure 4-16, the peak pressures of all three motored pressure traces occur one increment before TDC.

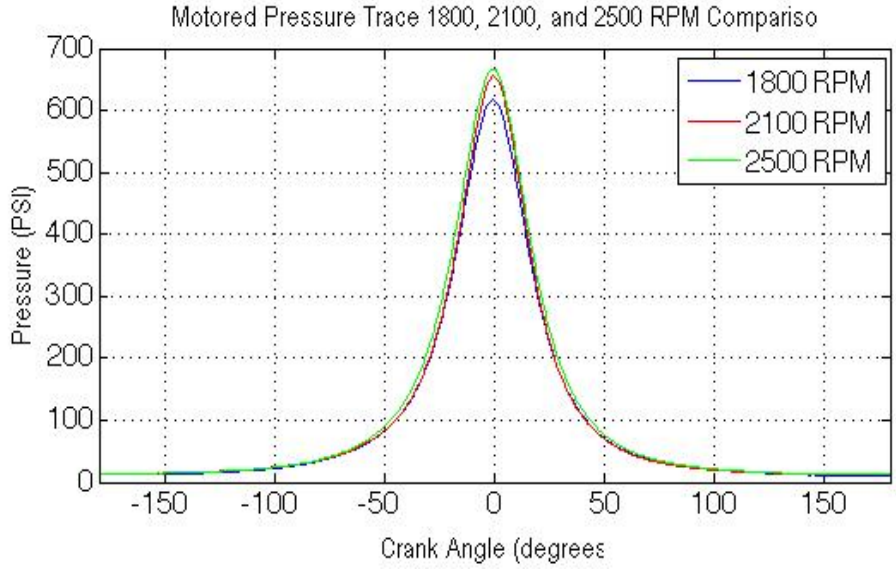

Figure 4 - 16: Comparison of Motored Plots for Different Engine Speeds

The next step is to plot a P-V diagram of the motored data. A P-V diagram is useful in verifying correct pressure-volume phasing. If the pressure data is correctly phased, there will be no crossing point between the compression and expansion curves. Figure 4-19 shows a zoomed view of the pressure-volume curve near TDC. There is no crossing point between the compression and expansion parts of the curve, and this is also the case for the other two conditions.

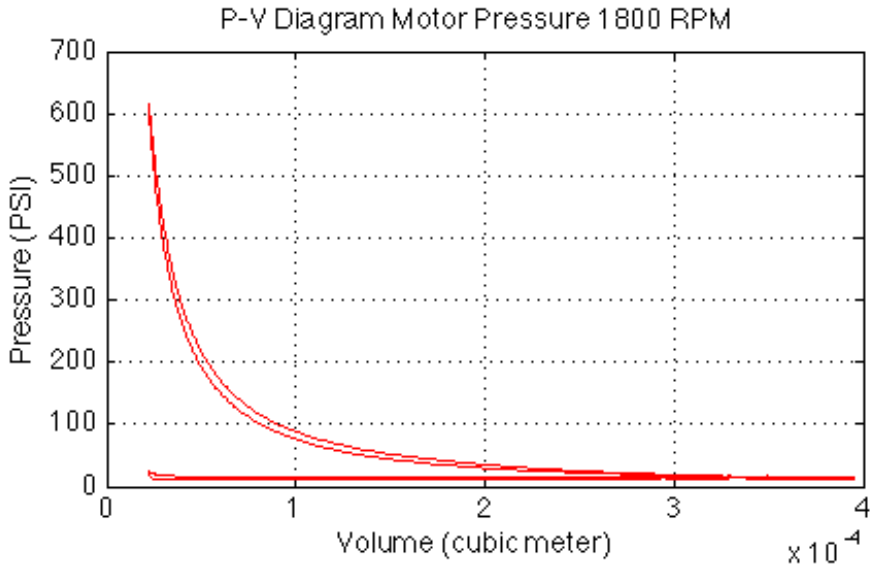

Figure 4 - 17: P-V Diagram for Motored Pressure Trace at 1800 RPM

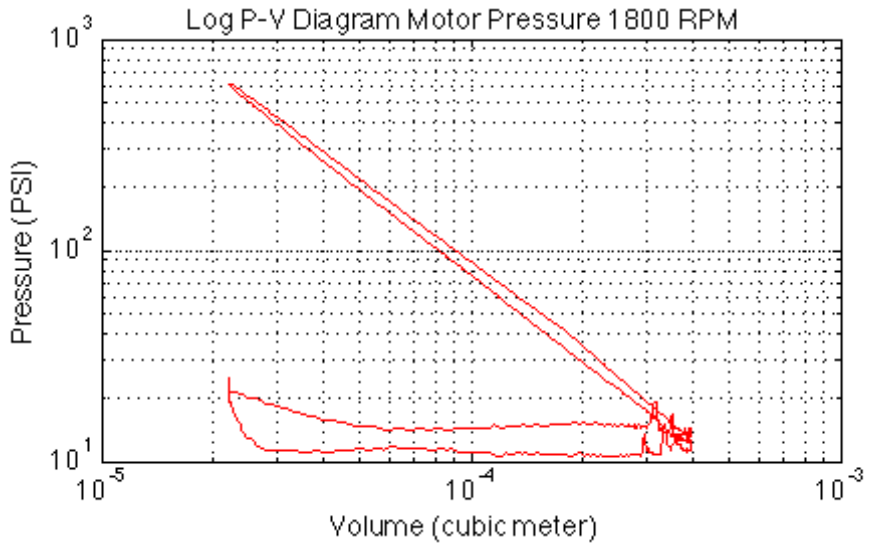

Figure 4 - 18: Log P-V Diagram of Motored Pressure Trace at 1800 RPM

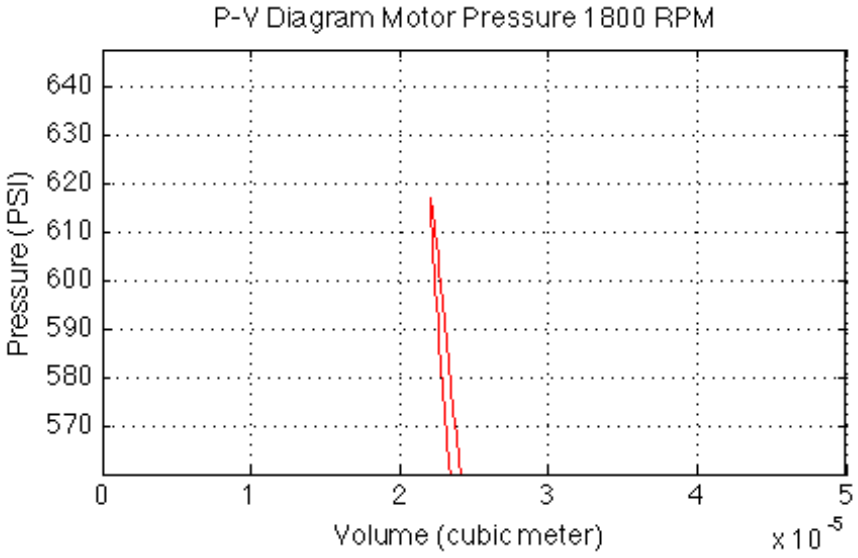

Figure 4 - 19: Zoom View of Crossing Point of P-V Diagram

The logarithmic P-V diagram is useful in determining correct reference pressure assignment and clearance volume assignment. If the reference pressure is not set correctly, there will be a slight curvature in the compression line near the first part of the stroke. The reference pressure is chosen by the pegging process described in the previous section. The average value for IMAP during the test run is assigned as the reference

pressure at BDC of the intake stroke. If the wrong clearance volume is assigned, then there will be a slight curvature in the compression line near TDC. As can be seen in Figure 4-18, the compression line is relatively flat. The compression curve, from IVC until near TDC, can also be approximated by the polytropic process.

$$PV^n = \text{constant} \tag{4.1}$$

This function plots as a straight line on the logarithmic diagram with slope equal to -n. Values of n range from 1.25 to 1.4. The slope of the compression line on the logarithmic p-V diagram should fall within this range of n values. One final test of the motored pressure data is a direct comparison with a simulation of the compression-expansion process of a motored engine. A simplified version of the main Matlab program has been created to model a motored pressure trace. The first law equation has been arranged to solve for pressure.

$$\frac{dP}{d\theta} = -\left(\frac{\gamma}{V}\right) p \frac{dV}{d\theta} - \left(\frac{\gamma - 1}{V}\right) \frac{dQ_{ht}}{d\theta} \tag{4.2}$$

The comparison for between the measured and estimated motor pressure trace at 2100 RPM can be seen in Figure 4-20. This condition had the most discrepancy between measured and simulated values. The main differences in measured and simulated pressure values occur at the peak value and during expansion.

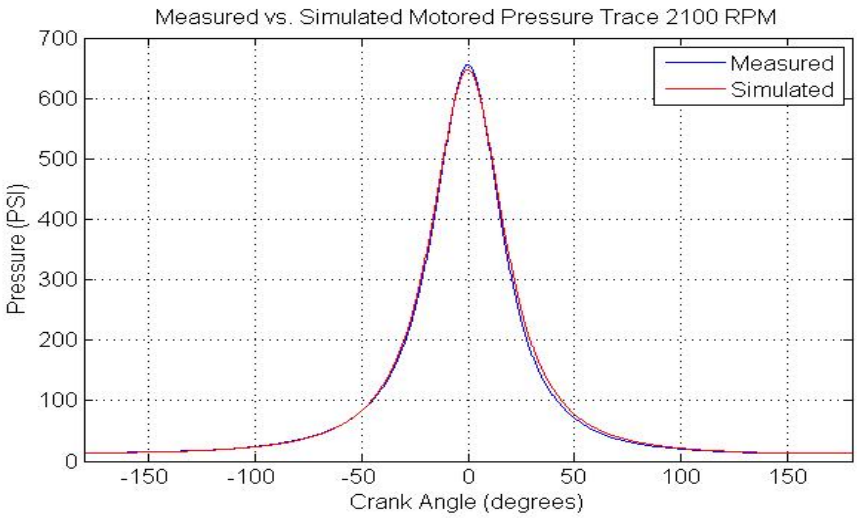

Figure 4 - 20: 2100 RPM Motored Comparison with Model

The difference between the measured and ideal pressure traces during the expansion stroke is due mainly to the heat transfer estimation with the Woschni model. At this point, the pressure-volume phasing, reference pressure, and clearance volume are correct and have been verified by simulated motored pressure traces. It is now time to move on to fired pressure data.

4.7 Data Filtering

The pressure transducer can be susceptible to signal noise from thermal shock and other issues described in the previous sections. A Matlab filtering function, 'filtfilt', is used to clean up signal noise. The function filters the data in the forward direction and then the filtered sequence is reversed and run through the filter again. This results in no phase distortion and a magnitude that is the square of the filter's magnitude response. The function also minimizes start-up and ending transients by matching initial conditions [16]. The coefficients of a low pass Butterworth filter design are applied to the double

filter function. The filtering process is similar to the one used by Gong [10]. The noise frequency of the pressure signal at 2500 RPM is around 6 to 7 crank angle, so an overall reduced frequency is set at

$$f_r = \frac{f_{data}}{\left(\frac{f_{sampling}}{2}\right)} = \frac{\left(\frac{1}{6.5}\right)}{\left(\frac{1}{2}\right)} = 0.308 \tag{4.3}$$

Therefore a reduced frequency around 0.30 is applied to the low pass Butterworth filter. The net heat release rate can be calculated using Equation 3.6

$$\frac{dQ_n}{d\theta} = \left(\frac{\gamma}{\gamma - 1}\right) p \frac{dV}{d\theta} + \left(\frac{1}{\gamma - 1}\right) V \frac{dp}{d\theta}$$

It is inevitable that differentiating the pressure data will increase noise in the equation above. In order to minimize the effects, the pressure data is filtered as described above and a fourth order central difference scheme is used

$$\frac{dP}{d\theta} = \frac{P_{i-2} - 8P_{i-1} + 8P_{i+1} - P_{i+2}}{12\Delta\theta} \tag{4.4}$$

The goal of filtering Eq (4.4) is to reduce the noise, specifically around the start and end of the compression and expansion strokes, respectively. However, too low of a reduced frequency leads to a reduced peak value and a phase shift. This would be unacceptable since we are using the main combustion peak to fit the shape factors. Following the approach presented by Gong [10], the pressure data is filtered at a lower reduced frequency up to SOI, and this same reduced frequency is used after the start of the main combustion. A higher reduced frequency is used between the first SOI and the main SOC to prevent any shifting of SOC points. Filtering the main combustion peak has little effect

on the burned mass estimation. A comparison of the different filter orders can be seen in Figure 4-22. The reduced frequency of 0.20 has a negative effect on the magnitude of the main combustion peak, but is able to suppress the noise seen during compression and expansion. The reduced frequency of 0.30 has no effect on the main peak, but there is still noise at the beginning and end of the crank period.

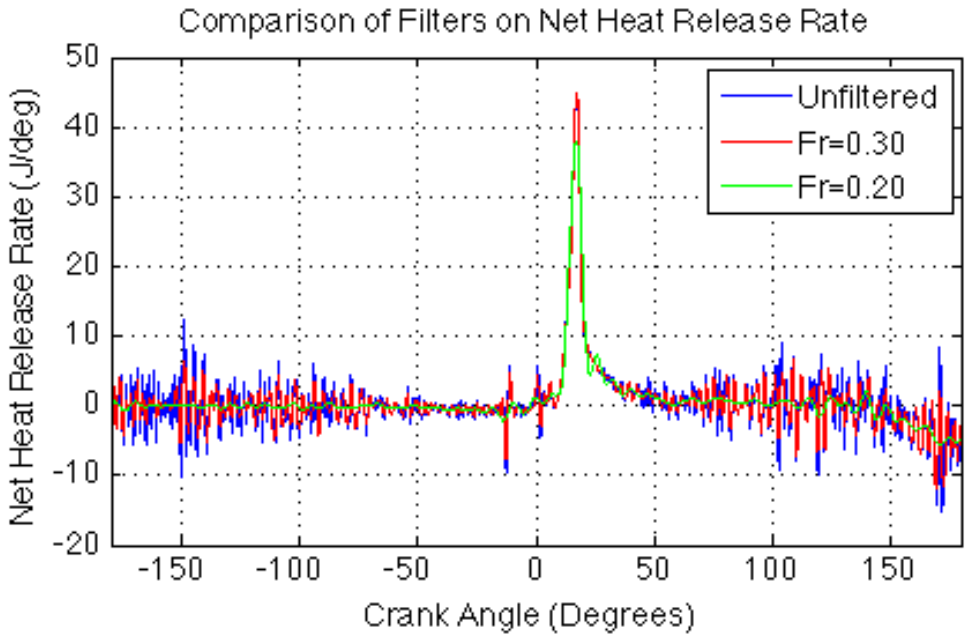

Figure 4 - 21: Filtered Net Heat Release Rate comparison

Using the lower reduced frequency for the beginning and end of the crank period yields the following result:

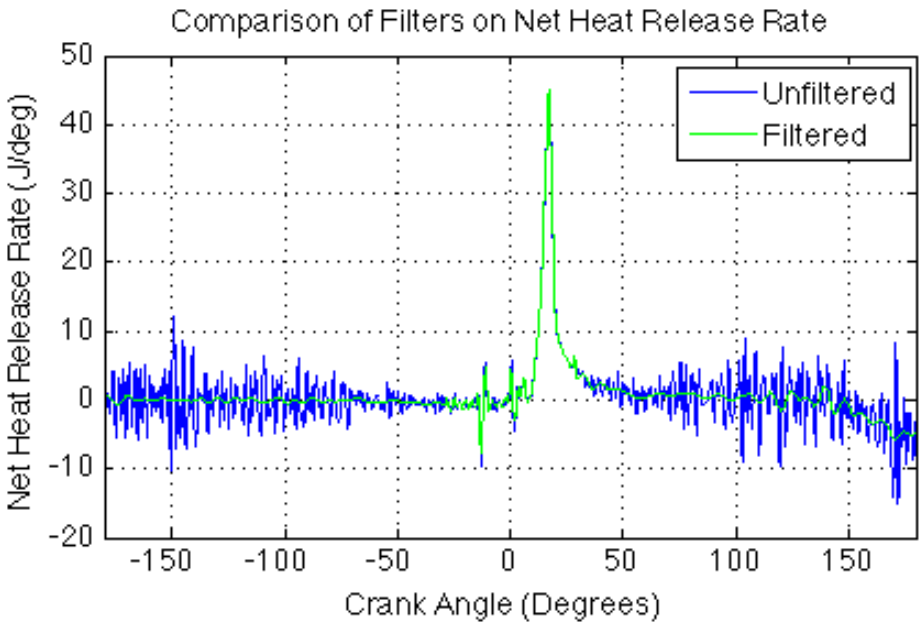

Figure 4 - 22: Net Heat Release Rate Raw vs. Filtered

The pressure traces of the filtered and unfiltered data can be seen in Figure 4-23. The changes between the filtered and unfiltered pressure traces are minimal and can mostly be seen at the beginning during intake, exhaust, and the peaks of the combustion points:

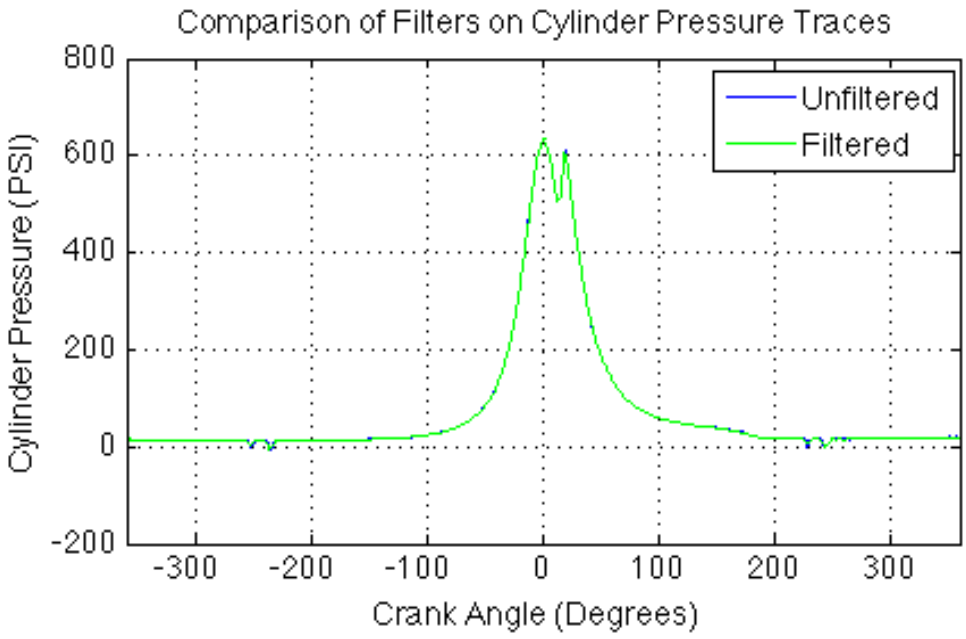

Figure 4 - 23: Pressure Trace Raw vs. Filtered

The filtered pressure traces are individually reviewed for each test condition.

4.8 Experimental Pressure Analysis Program

A diagram of the pressure analysis program can be seen in Figure 4-29. This program imports the cylinder pressure, injector current, and fuel rail pressure arrays from LabVIEW and then adjusts the cylinder pressure signal using the process described above. The injector current and the fuel rail pressure signals are averaged to correspond with the cylinder pressure signal. The fuel rail pressure voltage is also scaled to a specified pressure value [PSI]. Adjusted pressure files are created for motored and fired data. These pressure files are then combined with initial operating conditions to input into a governing equation model that is very similar to the one presented in Figure 3-1. The heat transfer, engine geometry, and properties models are the same as Figure 3-1, but the pressure differential, given in Eq. (4.4), is used to calculate the net heat release rate, $\frac{dQ_n}{d\theta}$. The outputs include crank position based plots of cylinder pressure, injector current, fuel rail pressure, net heat release rate, and cumulative heat release. P-V and log P-V diagrams are also generated. Overall cycle measurements like indicated work, IMEP, indicated torque, and ISFC are also calculated. The main purpose of this program is to generate the net heat release rate of the experimental pressure data, which will be used to calibrate the heat release model in the next chapter. Valuable information about the combustion during the test condition can also be gained by reviewing the P-V diagram and overall cycle measurements. Some of the outputs can be seen below in Figures 4-24 through 4-28 for a test condition at 2100 RPM and 62.5% Load.

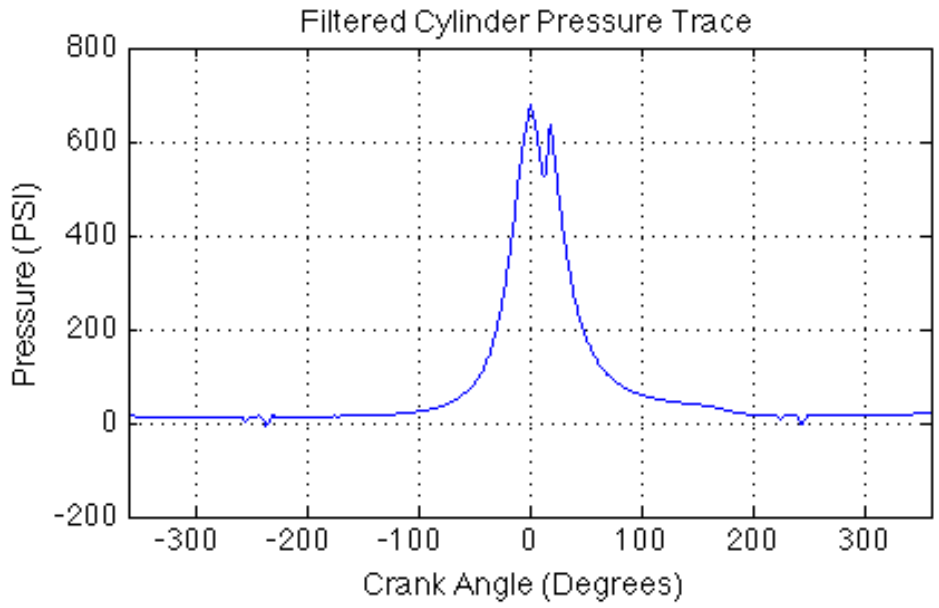

Figure 4 - 24: Filtered Pressure Output

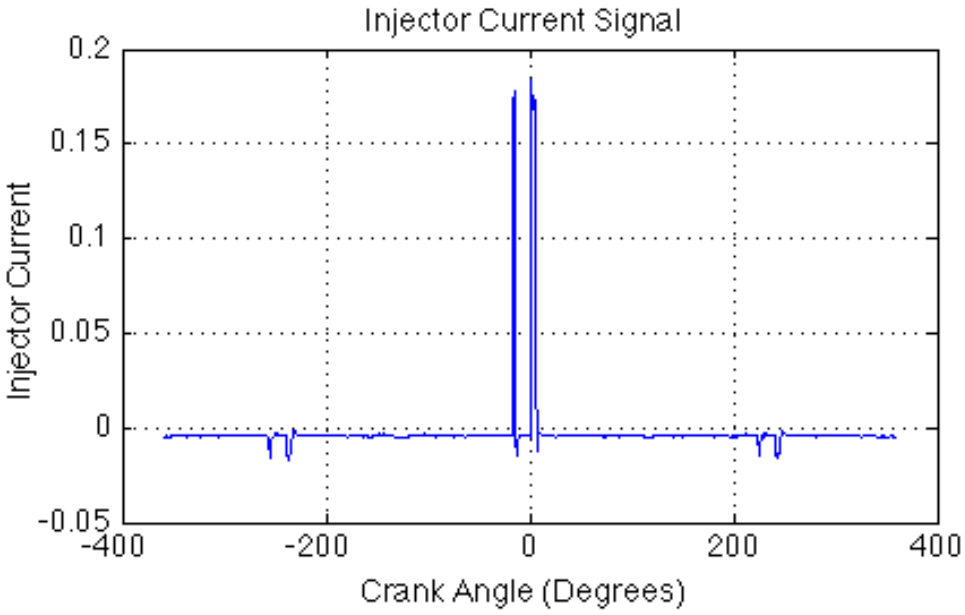

Figure 4 - 25: Injector Current Signal Output

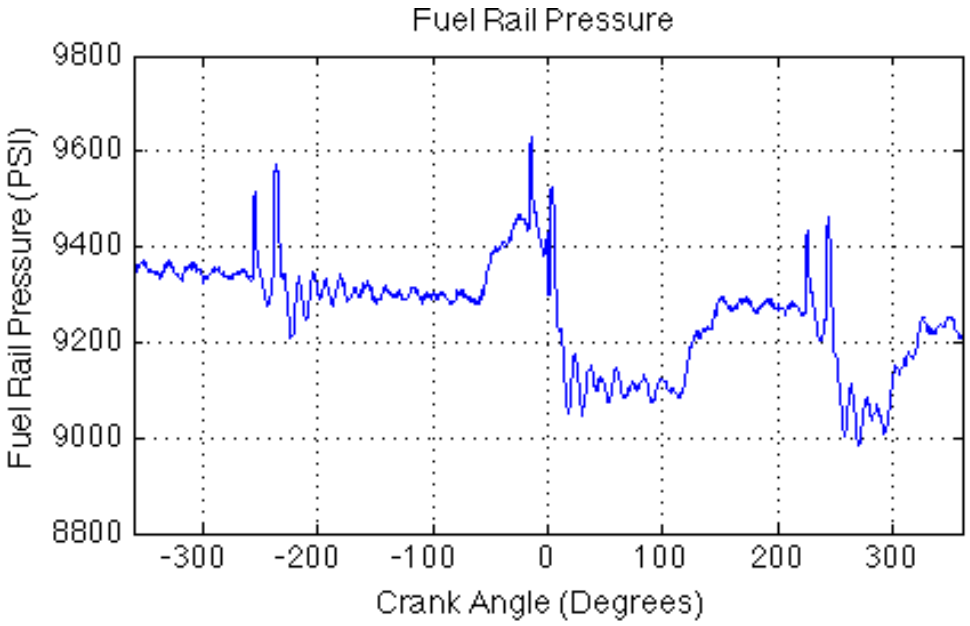

Figure 4 - 26: Fuel Rail Pressure Output

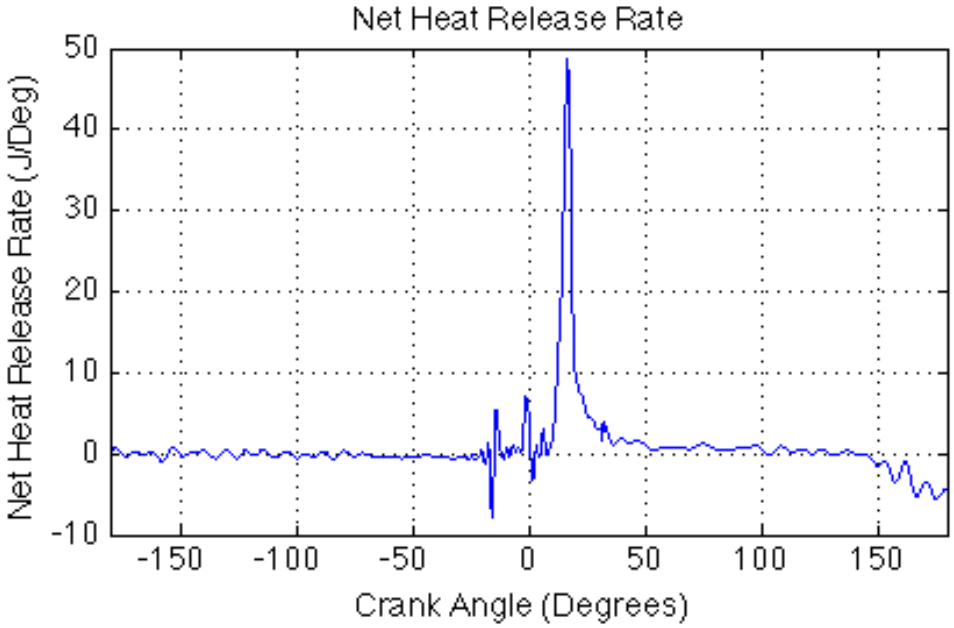

Figure 4 - 27: Net Heat Release Rate Output

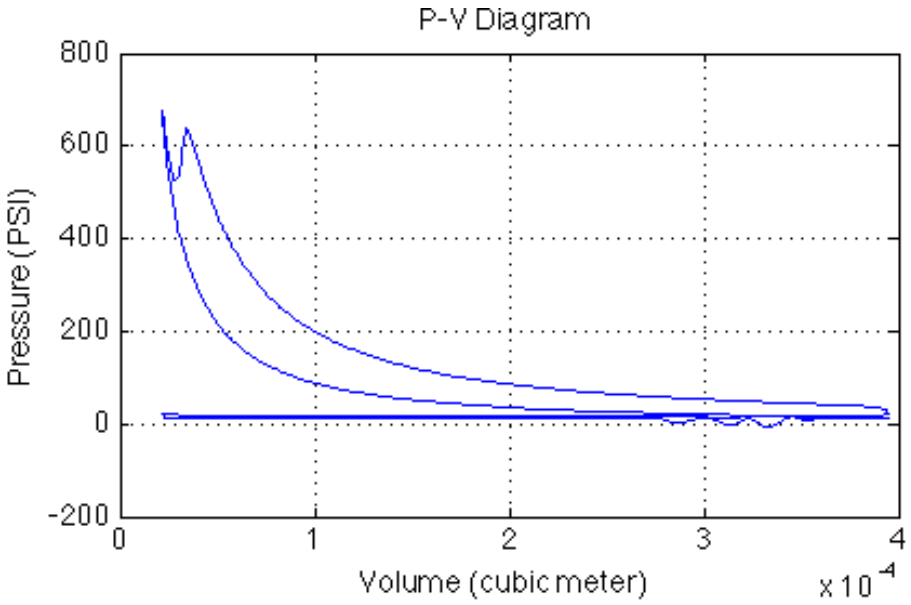

Figure 4 - 28: P-V Diagram Output of Experimental Pressure Analysis Program

Analyzing the cylinder pressure, injector current, net heat release rate, and fuel rail pressure on a common crank angle basis gives a good indication of the injection and combustion timing events during the cycle. The P-V diagram provides the necessary information to determine the overall cycle measurements. The cycle measurements for this test condition, 2100 RPM and 62.5% load, can be seen in Table 4-4.

Measurement	Value
Indicated Work	139.443 lb-ft
IMEP	73.4185 PSI
Indicated Torque	33.27 lb-ft
Dynamometer Torque	27.40 lb-ft
ISFC	0.3896 lbm/hp·h

Table 4 - 4: Overall Cycle Measurements for Test Condition

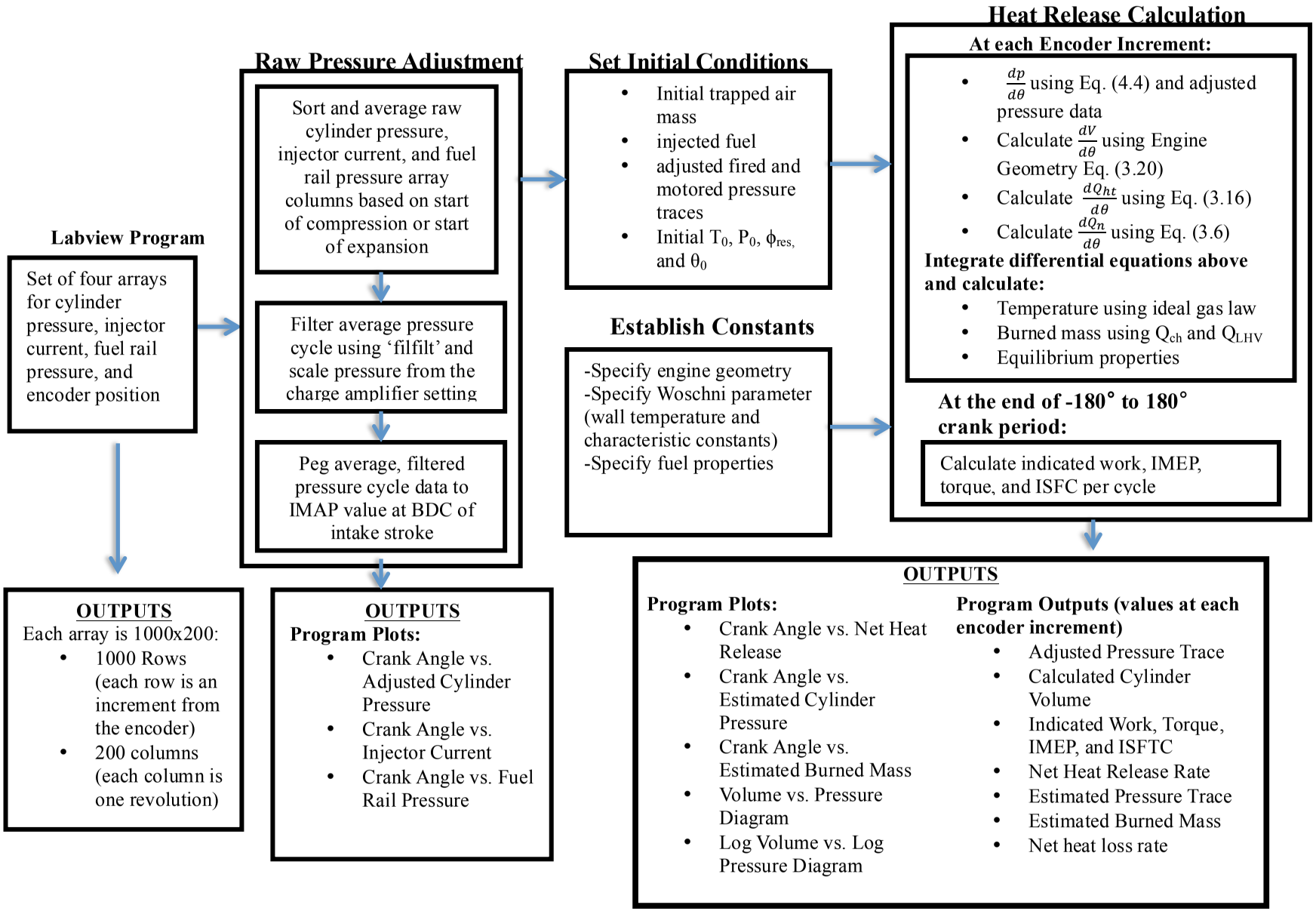

Figure 4 - 29: Diagram of the Matlab program to analyze the experimental pressure data

Chapter 5: Parameter Identification

5.1 Design of Experiment

A summary of the engine test conditions can be seen below. Tests were completed at 1800, 2100, and 2500 RPM. Data were taken at three different load values at each engine speed: 50%, 62.5%, and 75% load. The load is the calculated load value given from the ECU. The maximum load value is 75% in order to prevent any error due to thermal shock. A motored condition was recorded at each engine speed followed by the three specific load conditions. The pressure transducer was checked for drift before each motored condition. The test procedure and subsequent test results for each engine speed condition can be seen below:

START-UP/WARM-UP	
1	Calibrate injector current amplifier, wideband O_2 sensor, and dynamometer strain gage
2	Launch LabVIEW and other engine monitoring programs
3	Open water valves for engine cooling and dynamometer load. Turn on exhaust fan and cooling fans
4	Warm engine up to 185ºF ECT and under 80ºF IAT
5	Shut down engine
MOTORED TRACE	
6	Unplug fuel injector wire for #1 cylinder
7	Start engine and engine monitoring programs. Motor engine at specified RPM
8	Run the high speed LabVIEW program to record 8 runs once engine is at warm-up
9	Shut off engine and attach fuel injector wire to #1 cylinder
TEST	
10	Start engine and bring it up to the specified engine speed and 50% load. Start engine monitoring program
11	Run the high speed LabVIEW program to record 8 runs once engine has reached a steady condition
12	Proceed to the next to load conditions and record 8 runs once engine has reached a steady condition
13	Shut down engine
14	Start data analysis outlined in Chapter 4

Table 5 - 1: Engine Test Procedure

5.2 Fuel Injection Modeling

The fuel injection rate can be approximated by the one-dimensional flow presented by Assanis [9]:

$$\dot{m}_f \left[\frac{g}{s}\right] = C_D A_n \sqrt{2\rho_f \Delta P} \tag{5.1}$$

The discharge coefficient, C_D, is specific to the fuel injector design and is defined by Bosch to be 0.7. The nozzle area, A_n, can be calculated since it is known that the injectors have 7 holes, each with a diameter of 0.119 mm. The fuel density is taken to be a constant value at $\rho_f = 832$ g/m^3. ΔP is the difference between the fuel rail pressure and the cylinder pressure. Since the fuel rail pressure is so much larger than the cylinder pressure, an average cylinder pressure value of 750 PSI is assumed. Eq. (5.1) can also be converted to find the total fuel injected mass:

$$m_f [g] = C_D A_n \sqrt{2\rho_f \Delta P} \frac{\Delta\theta}{6N} \tag{5.2}$$

Net heat release rate curves were calculated for each test condition using the experimental pressure analysis program discussed in the previous chapter. These rate curves can be integrated to find the cumulative heat release over the given crank period. Using Eq. (3.2) and Eq. (3.6), the burned mass can be estimated from the cumulative gross heat release, which is a function of the net heat release and heat loss to the cylinder. According to Heywood [3], the estimated burned mass should be a decent approximation of the total fuel mass burned, depending on the accuracy of the heat transfer model. While this is not a direct validation of the fuel injection model, it does show that the widely accepted one-dimensional flow fuel injection model is sufficient for relatively simple single zone combustion models. The comparison between the estimated burned

mass and the estimated fuel injected can be seen in Table 5-2.

Test No.	Load %	RPM	Fuel Rail Pressure [PSI]	$\dot{m}_{f,inj}$ [g/s]	$m_{f,inj}$[g]	$m_{f,b}$ [g]	Error [%]
1	50	1833	8860.37	17.327	0.008507	0.008559	0.60
2	50	1845	8974.88	17.439	0.008507	0.008294	2.57
3	62.5	1812	8478.01	16.946	0.010662	0.010242	4.09
4	62.5	1805	8383.70	16.851	0.010643	0.010292	3.41
5	75	1766	8892.28	17.358	0.012974	0.012821	1.20
6	75	1763	9019.91	17.483	0.013090	0.012910	1.39
7	50	2140	8966.26	17.430	0.007819	0.007755	0.83
8	50	2117	9025.17	17.488	0.007930	0.007752	2.30
9	62.5	2087	9371.26	17.822	0.010247	0.009714	5.49
10	62.5	2080	9402.11	17.851	0.010299	0.009874	4.30
11	75	2100	10177.68	18.577	0.013033	0.013168	1.03
12	75	2105	10150.59	18.552	0.012985	0.013212	1.72
13	50	2445	12817.51	20.858	0.010749	0.009589	6.76
14	50	2430	11134.56	19.435	0.009597	0.009081	5.69
15	62.5	2498	10941.73	19.265	0.012956	0.012562	3.14
16	62.5	2495	10937.52	19.261	0.012506	0.012487	0.16
17	75	2522	13546.55	21.445	0.015816	0.016663	5.08
18	75	2543	13610.37	21.496	0.015722	0.016705	5.88

Table 5 - 2: Fuel Injection Model Approximation

The next step is to use the injector delay estimation equation below to find the dynamic start of injection.

$$t_d[\text{ms}] = 0.4815 - 0.0001313P_r - 0.00024P + 0.2 \qquad (5.3)$$

The injection delay, t_d, is applied to the SOI given by the ECU. The injection timing for all of the injections for the test conditions given in Table 5-2 can be seen below in Table 5-3. The injection timing values are given in degrees with respect to TDC = 360°. SOI and EOI are determined from the injector current signal graph in Figure 4-26. The dynamic SOI is the sum of the SOI position given by the injector current signal (ECU) and the injector delay (converted to degrees). SOC is estimated using a combination of the crank angle position vs. cylinder pressure graph, shown in Figure 4-25, and the net heat release rate curve, shown in Figure 4-28. The first pilot injection SOC is most easily determined by comparing the fired and motored cylinder pressure traces, shown in Figure

1-2. The separation of the fired and motored traces will be the location of the first SOC, as shown in Figure 5-1.

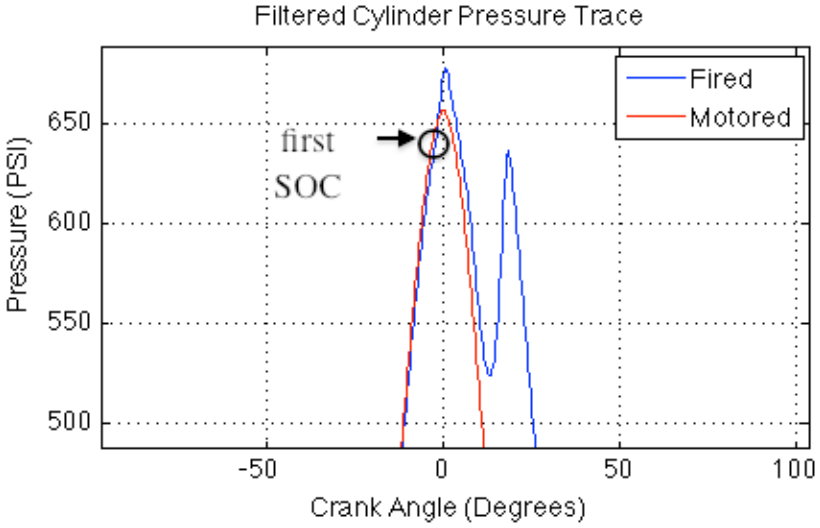

Figure 5 - 1: Location of first SOC

The start of combustion for the main injection can be located with the net heat release rate curve. Combustion begins with the heat release rate cross from negative to positive for the main injection peak. This location can be seen in Figure 5-2.

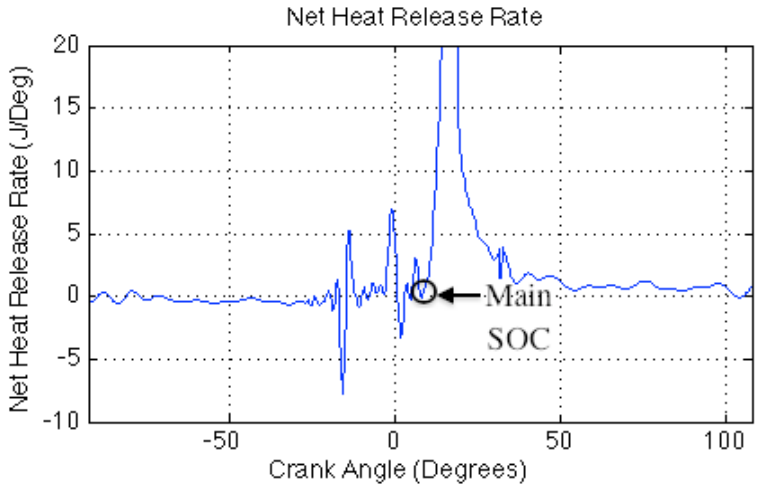

Figure 5 - 2: Location of Main SOC

Lean operating parameters, such as IMAP, MAF, and overall Ø, are also included.

Test No	SOI $(po)_1$ ECU	EOI $(po)_1$ ECU	SOI $(po)_1$	EOI $(po)_1$	SOC $(po)_1$	SOI $(po)_2$ ECU	EOI $(po)_2$ ECU	SOI $(po)_2$	EOI $(po)_2$	SOC $(po)_2$	SOI Main ECU	EOI main ECU	SOI main	EOI main	SOC main	MAF [lb/ min]	ø
1	346.7	349.2	352.1	354.6	356.8	-	-	-	-	-	360.7	366.8	366.1	371.5	369.4	1.32	0.598
2	346.7	349.2	342.1	354.1	356.8	-	-	-	-	-	360.7	366.8	366.1	371.5	369.4	1.35	0.602
3	346	349.2	351.3	354.6	356	-	-	-	-	-	360.4	367.2	365.7	372.6	369	1.42	0.679
4	346	349.2	351.3	354.5	356	-	-	-	-	-	360.4	367.6	365.7	372.5	369	1.41	0.671
5	346	348.1	350.4	353.3	353.9	-	-	-	-	-	359.6	367.6	364.8	372.7	366.5	1.66	0.710
6	345.3	348.1	350.4	353.3	353.9	-	-	-	-	-	359.6	367.6	364.8	372.7	366.5	1.66	0.713
7	345.3	347.4	349.4	353.7	357.8	-	-	-	-	-	360	366.8	366.3	372.4	370.1	1.65	0.524
8	343.1	347.4	349.3	353.6	357.8	-	-	-	-	-	360	366.8	366.2	372.3	370.1	1.63	0.525
9	343.1	346.7	348.8	352.7	356	-	-	-	-	-	360	367.2	366.1	373.3	369.7	1.71	0.616
10	342.7	346.7	348.4	352.7	356	-	-	-	-	-	360	367.2	366	373.2	369.7	1.74	0.625
11	342.4	345.2	347.3	351.3	351.4	-	-	-	-	-	360	368.6	366	374.9	367.9	2.16	0.717
12	341.3	345.6	347.3	351.6	351.7	-	-	-	-	-	360	368.6	366	374.9	367.9	2.18	0.721
13	341.3	343.1	345.1	349.7	357.8	-	-	-	-	-	358.2	366.1	364.9	372.4	367.6	2.25	0.500
14	341.3	343.1	345.2	349.9	357.8	-	-	-	-	-	358.2	366.5	365	372.2	367.6	2.20	0.501
15	315.2	319	321.3	326	337.3	334.4	338.8	341.5	345.8	351.7	356.1	366.1	363.1	373.2	364.7	2.73	0.650
16	315.2	319	321.3	326	337.3	334.1	338.8	341.1	345.8	351.7	356.1	365.8	363.1	372.8	364.7	2.73	0.646
17	314.3	318.2	320	325	336.6	333.0	337.7	339.8	344.4	349.9	355.7	366.5	362.4	373.6	364	3.20	0.725
18	314.3	318.2	320.4	325.1	336.6	333.4	337.7	340.2	344.5	349.9	355.7	366.5	362.5	373.7	364	3.24	0.722

Table 5 - 3: Injection Timing and Mean Operating Parameters of the Test Conditions

5.3 Heat Release Rate Estimation Model

5.3.1 Heat Release Rate Estimation Model Equations

The AFBR can be estimated using Watson's correlation

$$\frac{m_{f,b}(\tau)}{m_{f,inj}} = \beta\left(1-\left(1-\tau^{C_1}\right)^{C_2}\right) + (1-\beta)[1-e^{(-C_3\tau^{C_4})}] \qquad (5.4)$$

Where: $\tau = \frac{\theta-\theta_{ig}}{\Delta\theta_b}$ is the dimensionless time from ignition

The burn duration period is given by $\Delta\theta_b = \theta_{end} - \theta_{ig}$ and is a function of engine speed and load. An arbitrary value is usually chosen for the burn period in the model. Experimental burn periods were around 50º CA. A burn period of 90º CA was chosen for this model to insure full combustion is captured in the estimation. In Equation (5.4), there are five shape factors that need to be calibrated: β, C_1, C_2, C_3, and C_4.

5.3.2 Explanation of Parameter Identification

Before any parameters are calibrated, Equation (5.1) will be checked to see if it is a suitable approximation for light duty diesel applications. The shape parameters will be fit to the main injection of each test case, since it has the most prominent effect on the heat release rate curve. A nonlinear curve fitting function in Matlab, 'lsqcurvefit', is used to find the best-fit values for the shape parameters. This function finds the best fit coefficient "x" for the equation F(x,xdata) by minimizing the least-squares value:

$$\min_x \frac{1}{2}\|F(x,xdata)-ydata\|_2^2 = \frac{1}{2}\sum_i (F(x,xdata_i)-ydata_i)^2 \qquad (5.5)$$

Where: x is a vector of the shape parameters
xdata is the independent variable, the crank position θ
ydata is the experimental pressure trace

The experimental pressure data is used to fit the coefficients instead of the derived heat release rate curve. The net heat release rate is too sensitive to changes in pressure, which could result in incorrect shape parameter terms. This is the result of estimating the differential pressure using Eq. (4.4). Also, the overall cycle test metrics described in Chapter 1, the indicated work, IMEP, and indicated torque, are based on the pressure traces. The error is calculated using the following relationships:

$$\varepsilon = X_{ESTIMATED} - X_{TEST} \tag{5.6a}$$

$$\text{Error [\%]} = \sqrt{\frac{\sum_i \varepsilon^2}{N}} \frac{1}{\bar{X}_{TEST}} \times 100 \tag{5.6b}$$

Where: X is the parameter being considered
N is the crank position duration
$\bar{X}_{TEST}$ is the average value of the test value

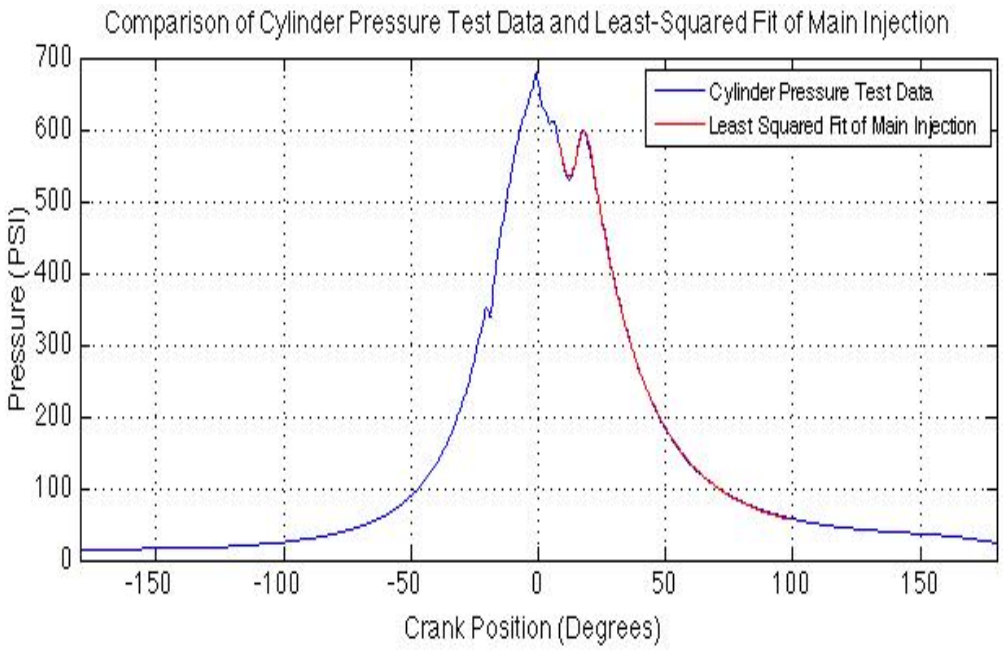

Figure 5 - 3: Least-Squared fit of main injection

The results of the least-squared fit of the pressure data can be seen in Figure 5-3. Watson's burned mass equation can be used to accurately predict the cylinder pressure

trace. There are only certain areas right after SOC and at the end of the burn period where the least squared fit slightly deviates from the test data. One point worth mentioning is that Watson presents the proportionality factor β and the diffusion controlled shape parameter C_3 as a function of the trapped equivalence ratio. This value can be reasonably estimated using Gong's injection delay correlation, but the installation of a needle lift sensor will provide the most accurate results. A summary of the parameter fit data for the test conditions can be seen in Table 5-4. The ignition delay, τ_{id}, is the time between SOC and the dynamic SOI. The trapped equivalence ratio is a function of the trapped fuel mass and the trapped air mass. The trapped air is estimated using Eq. (3.24). The trapped fuel mass is estimated using Eq. (5.2) and setting $\Delta\theta$ to the ignition delay value in degrees. The test values for the Watson shape parameters are calculated using the least squared fit method described above. The next section will review the method for tuning the shape parameters.

Test No	SOI Main ECU	EOI main ECU	SOI main	EOI main	SOC main	τ_{id} [ms]	Trapped ø	Test β	Test C_1	Test C_3	Test C_4	Tuned β	Tuned C_1	Tuned C_3	Tuned C_4
1	360.7	366.8	366.1	371.5	369.4	0.296	0.346	0.475	3.647	4.463	1.134	0.495	3.541	4.732	1.231
2	360.7	366.8	366.1	371.5	369.4	0.292	0.328	0.483	3.653	4.577	1.118	0.503	3.544	4.726	1.243
3	360.4	367.2	365.7	372.6	369	0.301	0.303	0.536	3.674	4.700	1.279	0.542	3.538	4.717	1.257
4	360.4	367.6	365.7	372.5	369	0.304	0.303	0.539	3.672	4.675	1.274	0.546	3.537	4.717	1.254
5	359.6	367.6	364.8	372.7	366.5	0.156	0.138	0.432	3.637	4.573	1.374	0.394	3.810	4.628	1.243
6	359.6	367.6	364.8	372.7	366.5	0.158	0.140	0.438	3.652	4.558	1.411	0.397	3.804	4.630	1.241
7	360	366.8	366.3	372.4	370.1	0.296	0.300	0.541	3.425	4.930	1.033	0.536	3.485	4.716	1.282
8	360	366.8	366.2	372.3	370.1	0.305	0.306	0.548	3.439	4.905	1.035	0.546	3.478	4.718	1.280
9	360	367.2	366.1	373.3	369.7	0.291	0.284	0.531	3.400	4.594	1.259	0.541	3.500	4.710	1.245
10	360	367.2	366	373.2	369.7	0.294	0.296	0.549	3.425	4.565	1.296	0.536	3.498.	4.714	1.242
11	360	368.6	366	374.9	367.9	0.151	0.132	0.348	3.477	4.401	1.265	0.383	3.751	4.624	1.223
12	360	368.6	366	374.9	367.9	0.149	0.131	0.352	3.475	4.413	1.284	0.379	3.755	4.623	1.225
13	358.2	366.1	364.9	372.4	367.6	0.184	0.170	0.455	3.712	5.150	1.473	0.430	3.611	4.652	1.306
14	358.2	366.5	365	372.2	367.6	0.173	0.160	0.484	3.687	5.213	1.418	0.410	3.638	4.645	1.312
15	356.1	366.1	363.1	373.2	364.7	0.106	0.086	0.238	3.896	4.821	1.269	0.282	3.829	4.576	1.270
16	356.1	365.8	363.1	372.8	364.7	0.106	0.089	0.230	3.901	4.783	1.249	0.272	3.827	4.580	1.266
17	355.7	366.5	362.4	373.6	364	0.100	0.084	0.181	4.101	4.298	1.183	02.46	3.849	4.574	1.212
18	355.7	366.5	362.5	373.7	364	0.096	0.083	0.178	4.109	4.232	1.183	0.218	3.863	4.572	1.204

Table 5 - 4: Watson Shape Parameter Least Square Fit Parameters

5.3.3 Burning mode factor β

Watson originally proposed that the proportionality factor be represented as

$$\beta = 1 - \frac{a_\beta \varphi_{ig}^{(b_\beta)}}{\tau_{id}^{c_\beta}} \tag{5.7}$$

Watson originally set the coefficients in Eq. (5.7) to $a_\beta = 0.95$, $b_\beta = 0.41$, and $c_\beta = 0.28$. β values for each test condition, shown in Table 5-4, are calculated using Eq. (5.7) and Watson's original coefficients. The test values for trapped equivalence ratio and ignition delay are also provided. These values are compared to the test β shape parameter value shown in Table 5-4. An error is calculated using Eq. (5.6b) and is given in Table 5-5.

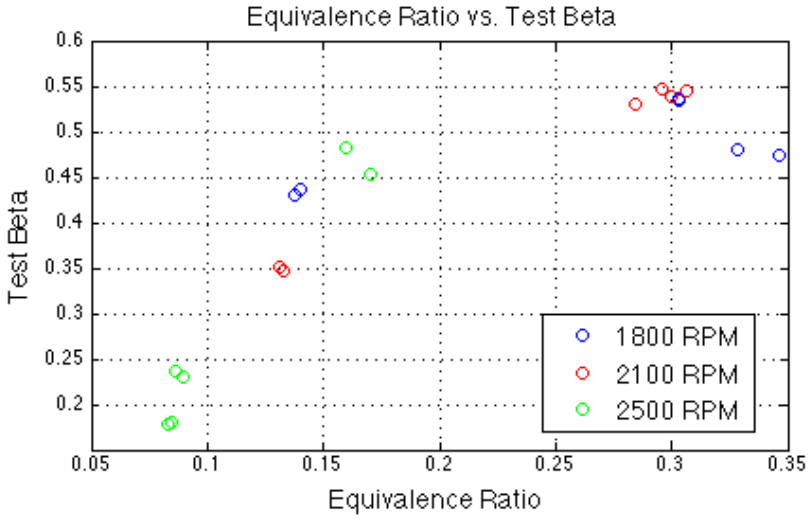

Figure 5 - 4: Effect of Equivalence Ratio on the Test Parameter Beta

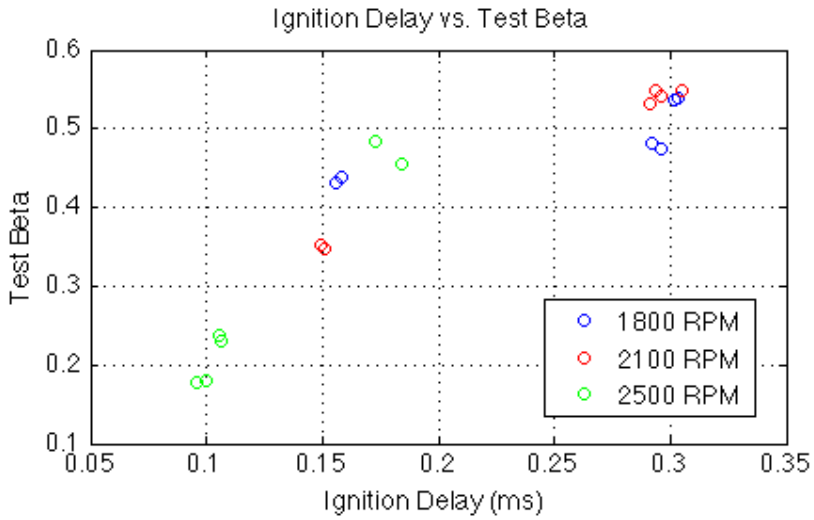

Figure 5 - 5: Effect of Ignition Delay on the Test Parameter Beta

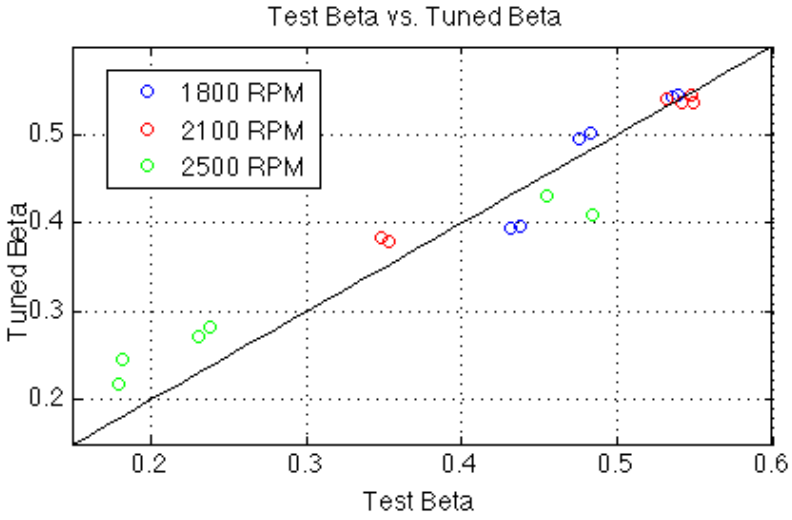

Figure 5 - 6: Comparison between Test Beta and Tuned Beta

The effect of the two inputs to β in Eq. (5.7), the trapped equivalence ratio φ_{ig} and the ignition delay τ_{id}, can be seen in Figures 5-4 and 5-5. Since the trapped fuel mass is related to the ignition delay, both graphs display similar trends over the different test conditions. The tuned β values have an acceptable error when compared to the test β values and the model has good agreement at all test points, as can be seen in Figure 5-6.

This is good since Watson emphasizes the importance of beta in shaping the heat release profile. The final equation for the estimating the weighting coefficient β can be seen below in Table 5-5.

Model	Equation	Error [%]
Untuned Watson	$\beta = 1 - \frac{0.95\varphi^{0.41}}{\tau_{id}{}^{0.28}}$	**57.63**
Tuned Watson	$\beta = 1 - \frac{0.365\varphi^{0.258}}{\tau_{id}{}^{1.442}}$	**8.31**

Table 5 - 5: Final Equation for β

5.3.4 Pre-mixed Shape Factors

Watson concluded that the shape factors C_1 and C_2 are used to control the timing and the slope of the rise and fall characteristic of the peak. C_1 is dependent upon the ignition delay and the engine speed. Watson's equation for predicting C_1 is

$$C_1 = 2 + a_{C_1}(\tau_{id}N)^{bc_1} \qquad (5.8)$$

Watson originally set the coefficients in Eq. (5.8) to $a_{C1} = 1.25 \times 10^{-8}$ and $b_{C1} = 2.4$. C_1 values for each test condition, shown in Table 5-4, are calculated using Eq. (5.8) and Watson's original coefficients. These values are compared to the test C_1 shape parameter value shown in Table 5-4. An error is calculated using Eq. (5.6b) and is given in Table 5-6.

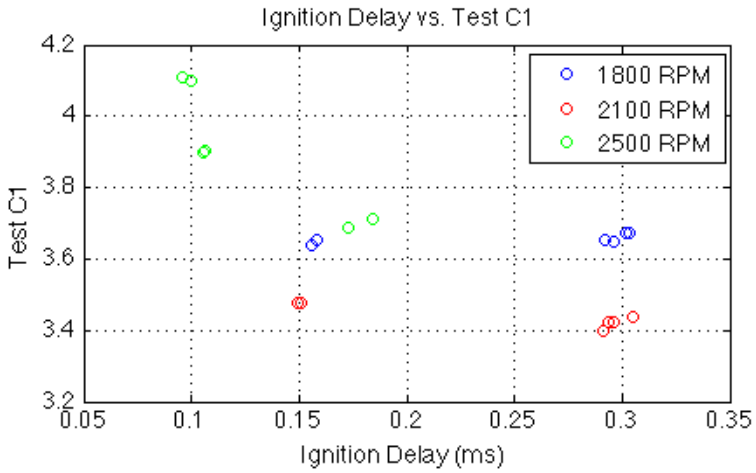

Figure 5 - 7: Effect of Ignition Delay on the Test Parameter C_1

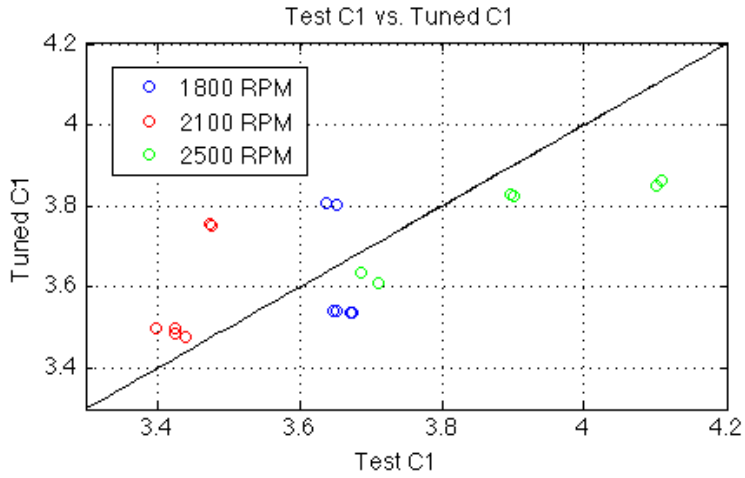

Figure 5 - 8: Comparison between Test C_1 and Tuned C_1

Figure 5-7 shows the comparison between the shape parameter C_1 and ignition delay. The shape parameter values at 1800 RPM and 2100 RPM follow a very similar trend, staying consistently around 3.45 and 3.65, respectively. The shape parameter increases as the ignition delay decrease for the 2500 RPM condition. Figure 5-8 shows a comparison between the test shape parameter and the tuned shape parameter. The approximation for C_1 is slightly less accurate than the approximation for β. Watson's

experimental results show that the shape of the peak improved with high values of C_2 up to 5000 with marginal benefits deviating from this point. Therefore, a value of 5000 is assigned to C_2 in this study. The final equation for the estimating the weighting coefficient C_1 can be seen below in Table 5-6.

Model	Equation	Error [%]
Untuned Watson	$C_1 = 2 + 1.25\times10^{-8}(\tau_{id}N)^{2.4}$	**45.01**
Tuned Watson	$C_1 = 2 + 15.353(\tau_{id}N)^{-0.306}$	**4.23**

Table 5 - 6: Final Equations for C_1

5.3.5 Diffusion Controlled Parameters

The shape factors C_3 and C_4 change the rate of diffusion and the timing of the peak burning diffusion rate, respectively. The shape factor is dependent on the trapped equivalence ratio, as can be seen in Watson's equation:

$$C_3 = \frac{a_{C_3}}{\varphi_{ig}{}^{bc_3}} \tag{5.9}$$

Watson originally set the coefficients in Eq. (5.8) to a_{C3} = 14.2 and b_{C3} = 0.644. C_3 values for each test condition, shown in Table 5-4, are calculated using Eq. (5.9) and Watson's original coefficients. These values are compared to the test C_3 shape parameter value shown in Table 5-4. An error is calculated using Eq. (5.6b) and is given in Table 5-7. Watson represents this shape parameter solely as a function of the trapped equivalence ratio.

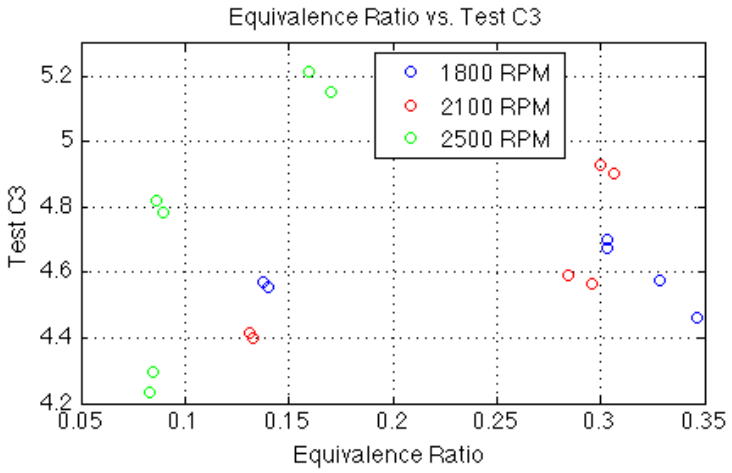

Figure 5 - 9: Effect of the Trapped Equivalence Ratio on C_3

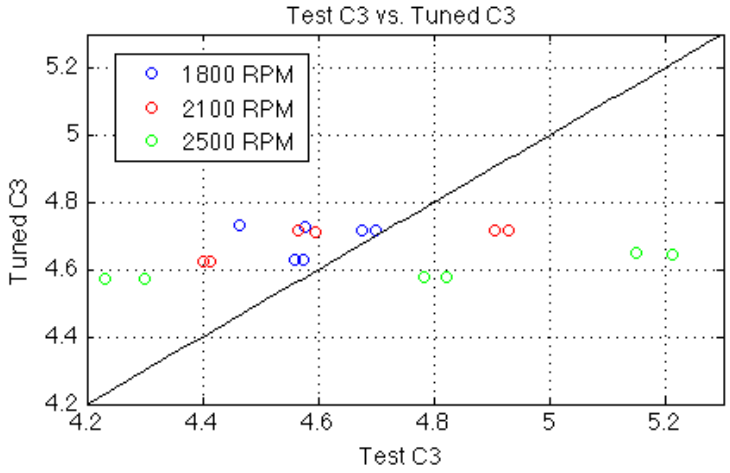

Figure 5 - 10: Comparison of Test Parameter C_3 and Tuned Parameter C_3

The effect of the trapped equivalence ratio on the shape parameter C_3 can be seen in Figure 5-9. As the test conditions increase from 1800 to 2500 RPM, the trapped equivalence ratio range decreases as the range of shape parameter values increases. The shape parameter values at 1800 RPM stay relatively constant around 4.6 while the trapped equivalence ratio has a small range between 0.6 and 0.72. This range decreases as the engine speed increases. The equivalence ratio range at 2500 RPM is between 0.08

and 0.16 for different load values, but the shape parameter varies from 4.2 to 5.2. Figure 5-10 shows a comparison between the test shape parameter and the tuned shape parameter. Despite the variation in test shape parameter values, the tuned shape parameter values at each engine speed stay relatively constant.

Watson notes the strong interaction between C_3 and C_4 as can be seen in the equation for C_4 :

$$C_4 = a_{C_4} C_3^{\,b_{C_4}} \qquad (5.10)$$

Watson originally set the coefficients in Eq. (5.10) to $a_{C4} = 0.79$ and $b_{C4} = 0.25$. C_4 values for each test condition, shown in Table 5-4, are calculated using Eq. (5.10) and Watson's original coefficients. These values are compared to the test C_4 shape parameter value shown in Table 5-4. An error is calculated using Eq. (5.6b) and is given in Table 5-7. Watson represents this shape parameter solely as a function of the test shape parameter C_3.

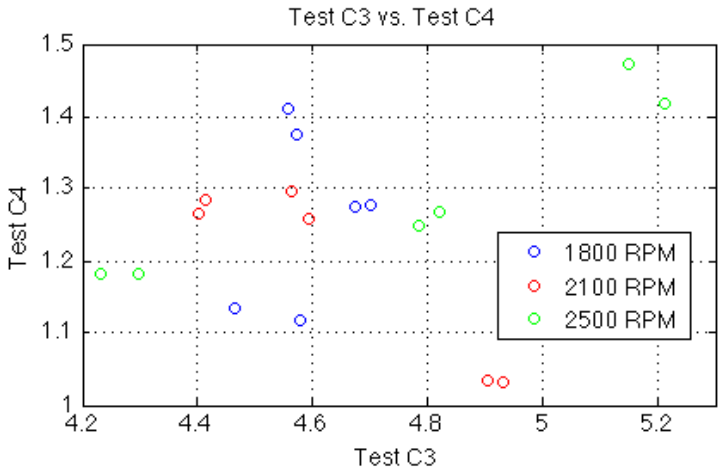

Figure 5 - 11: Effect of Test Shape Parameter C_3 on Test Shape Parameter C_4

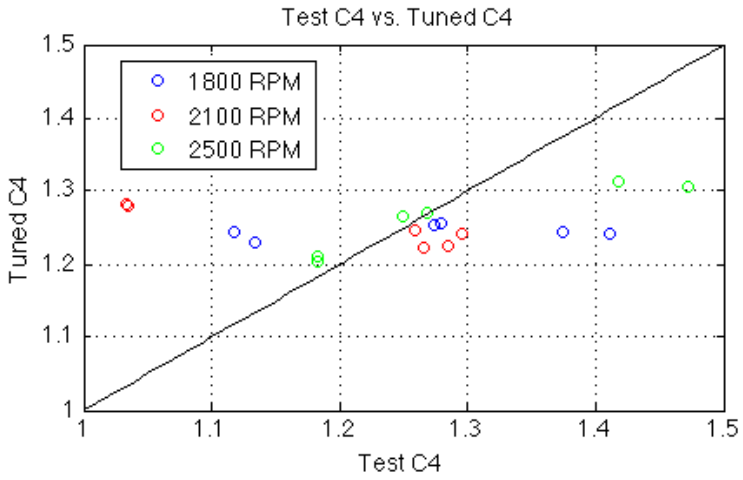

Figure 5 - 12: Comparison of Test Parameter C_4 and Tuned Parameter C_4

Figure 5-11 shows the relationship between the shape parameter C_3 and C_4. There doesn't seem to be a strong relationship between these parameters based on the test data. Figure 5-12 shows a comparison between the test shape parameter and the tuned shape parameter. The result is similar to the comparison between the test and tuned C_3 shape parameters. While the test shape parameter varies between 1.0 and 1.5, the tuned parameter stays fairly constant around 1.25 for all test conditions. The final equation for the estimating the shape parameters C_3 and C_4 can be seen below in Table 5-7.

Model	Equation	Error [%]
Untuned Watson	$C_3 = \frac{14.2}{\varphi^{0.644}}$	**>100**
Tuned Watson	$C_3 = \frac{3.93}{\varphi^{0.367}}$	**5.49**
Untuned Watson	$C_4 = 0.79{C_3}^{0.25}$	**>100**
Tuned Watson	$C_4 = 0.663{C_3}^{0.413}$	**9.28**

Table 5 - 7: Final Equations for shape parameters C_3 and C_4

Chapter 6: Model Validation

6.1 Overall Model Explanation and Flowchart

The addition of the heat release estimation model requires minor modification to the flowchart in Figure 4-29. Since the method for estimating the net heat release rate and pressure varies depending the engine cycle process, the model is divided into four parts: (1) Compression (BDC to the first SOC), (2) Pilot injections (first SOC to primary SOC), (3) Main Injection (primary SOC to the end of the burn period), and (4) Expansion (end of burn period to BDC). The equations for heat loss rate, work rate, and net heat release rate do not change between the parts of the model and are given below:

$$\frac{dQ_{ht}}{d\theta} = \frac{h_g(\frac{\pi B^2}{2} + \frac{4V}{B})(T_g - T_w)}{\omega} \tag{6.1}$$

$$\frac{dQ_n}{d\theta} = \left(\frac{\gamma}{\gamma - 1}\right) p \frac{dV}{d\theta} + \left(\frac{1}{\gamma - 1}\right) V \frac{dp}{d\theta} \tag{6.2}$$

$$\frac{dW}{d\theta} = p \frac{dV}{d\theta} \tag{6.3}$$

The compression and expansion models use the following equation to estimate pressure:

$$\frac{dP}{d\theta} = -\frac{\gamma}{V} p \frac{dV}{d\theta} - \frac{\gamma - 1}{V} \frac{dQ_{ht}}{d\theta} \tag{6.4}$$

Once pressure is estimated from Eq. (6.4), the net heat release rate can be calculated using Eq. (6.2). The combustion models use Watson's equation to estimate pressure:

$$\frac{dP}{d\theta} = \frac{\gamma - 1}{V}\left(\frac{dQ_{ch}}{d\theta} - \frac{dQ_{ht}}{d\theta}\right) - \frac{\gamma}{V}p\frac{dV}{d\theta} \tag{6.5}$$

After the core equations are integrated, other output values can be calculated at each integration step. The burned mass can be calculated from cumulative gross heat release, the temperature can be calculated from the ideal gas law, and the thermodynamic and equilibrium properties can be calculated using the adopted models from Olikara and Borman [11]. The gross heat release rate, $\frac{dQ_{ch}}{d\theta}$, for the pilot injection is estimated using Watson's model and the tuned parameter equations, Eqs. (5.7) through (5.10). The burn period is adjusted for the pilot injection. Shape parameters are calculated based on the trapped equivalence ratio, engine speed, and ignition delay for each pilot injection. The gross heat release rate for the main injection is estimated using the same model and values for trapped equivalence ratio, engine speed, and ignition delay. The following values are calculated at each increment: volume, pressure, temperature, γ, φ, net and gross heat release rate, net and gross heat release, heat loss rate, and work. The core differential equations are integrated with the same step value of the incremental encoder to provide the closest approximation to the test data. The modified heat release calculation, which can be substituted for the heat release calculation in Figure 4-29, can be seen in Figure 6-1.

Modified Heat Release Calculation

At each Encoder Increment:

Compression (-180° to first SOC)

- Calculate $\frac{dV}{d\theta}$ using Engine Geometry Eq. (3.18)
- Calculate $\frac{dQ_{ht}}{d\theta}$ using Eq. (6.2)
- $\frac{dp}{d\theta}$ using Eq. (6.4) and adjusted pressure data

Integrate differential equations above and calculate:

- Temperature using ideal gas law
- Equilibrium and Woschni properties

Pilot Combustion (first SOC to main SOC)

- Calculate $\frac{dV}{d\theta}$ using Engine Geometry Eq. (3.18)
- Calculate $\frac{dQ_{ht}}{d\theta}$ using Eq. (6.2)
- Calculate $\frac{dQ_{ch}}{d\theta}$ using Eqs. (3.7,3.8,3.9, and 3.10)
- $\frac{dp}{d\theta}$ using Eq. (6.5) and adjusted pressure data

Integrate differential equations above and calculate:

- Temperature using ideal gas law
- Equilibrium and Woschni properties

Main Combustion (main SOC to end of burn period)

- Calculate $\frac{dV}{d\theta}$ using Engine Geometry Eq. (3.18)
- Calculate $\frac{dQ_{ht}}{d\theta}$ using Eq. (6.2)
- Calculate $\frac{dQ_{ch}}{d\theta}$ using Eqs. (3.7,3.8,3.9, and 3.10)
- $\frac{dp}{d\theta}$ using Eq. (6.5) and adjusted pressure data

Integrate differential equations above and calculate:

- Temperature using ideal gas law
- Equilibrium and Woschni properties

Expansion (end of burn period to 180°)

- Calculate $\frac{dV}{d\theta}$ using Engine Geometry Eq. (3.18)
- Calculate $\frac{dQ_{ht}}{d\theta}$ using Eq. (6.2)
- $\frac{dp}{d\theta}$ using Eq. (6.4) and adjusted pressure data

Integrate differential equations above and calculate:

- Temperature using ideal gas law
- Equilibrium and Woschni properties

Figure 6 - 1: Modified Heat Release Rate Calculation Model

6.2 Test Condition 2250 RPM 62.5% Load

A test condition at 2250 RPM and 62.5% was chosen to validate the heat release estimation model. Figures 6-2, 6-3, and 6-4 give the crank angle based outputs for measured cylinder pressure, injector current, and fuel rail pressure.

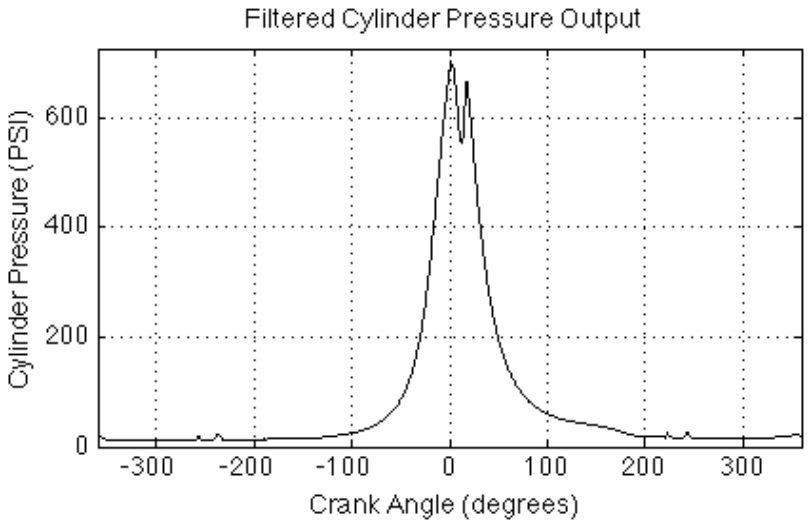

Figure 6 - 2: Cylinder Pressure Output for 2250 RPM and 62.5% Load

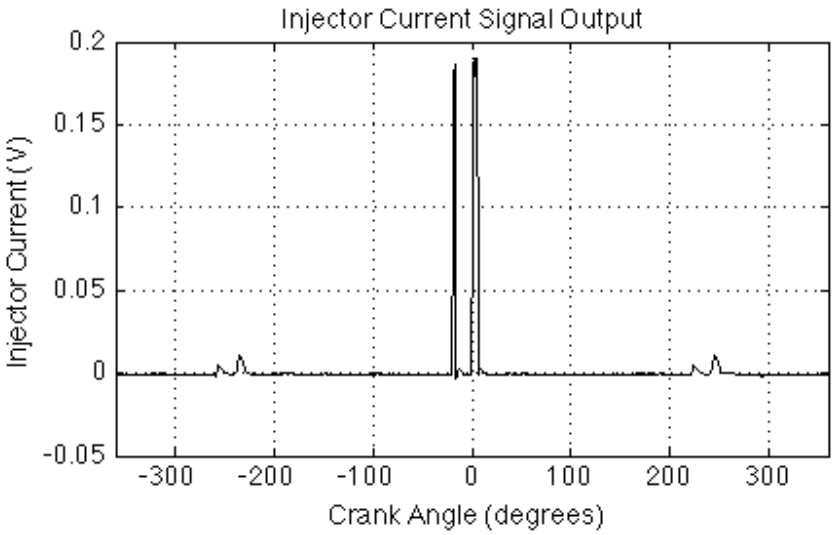

Figure 6 - 3: Injector Current Signal Output for 2250 RPM and 62.5% Load

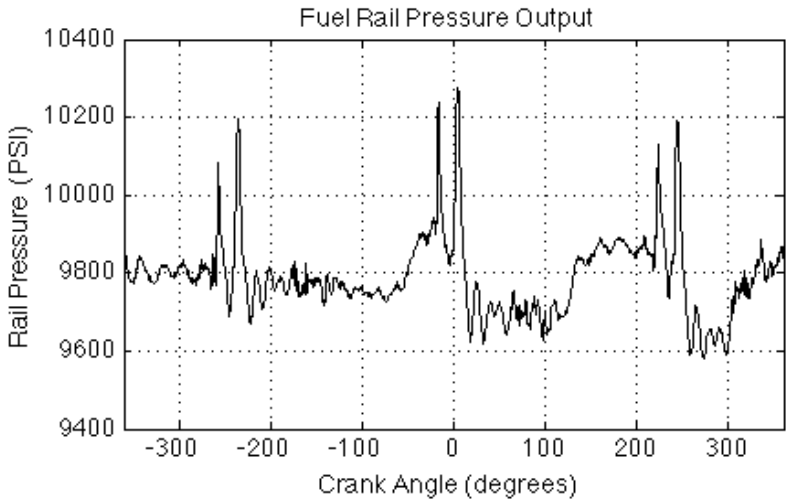

Figure 6 - 4: Fuel Rail Pressure Output for 2250 RPM and 62.5% Load

SOI, EOI, and SOC for the pilot and main injections can be determined from Figures 6-2 and 6-3, along with the net heat release rate from experimental pressure data. The injection delay, ignition delay, trapped air mass, fuel mass, and trapped equivalence ratio can all be calculated using a combination of the mean operating parameter recording and the outputs from the experimental pressure analysis program shown in Figures 6-2 through 6-4. Once this information is determined, the heat release model equations, Eqs (3.9, 5.7-5.10), can be calculated. It is now possible to run the overall model with the heat release estimation model, shown in Figure 6-1. Figures 6-5 through 6-8 show the comparison of the estimated values of the overall model with the measured values from the experimental pressure analysis program. As can be seen in Figure 6-5, there is an overestimation of pressure at the pilot injection. This overestimation leads to a separation between the measured and estimated pressure right before the main SOC, around 5° after TDC. The estimated pressure is a close approximation through main injection combustion, but there is also a slight overestimation at the main combustion peak. Using Eq. (5.6b), the error between the estimated pressure and the measured pressure is 8.91 %.

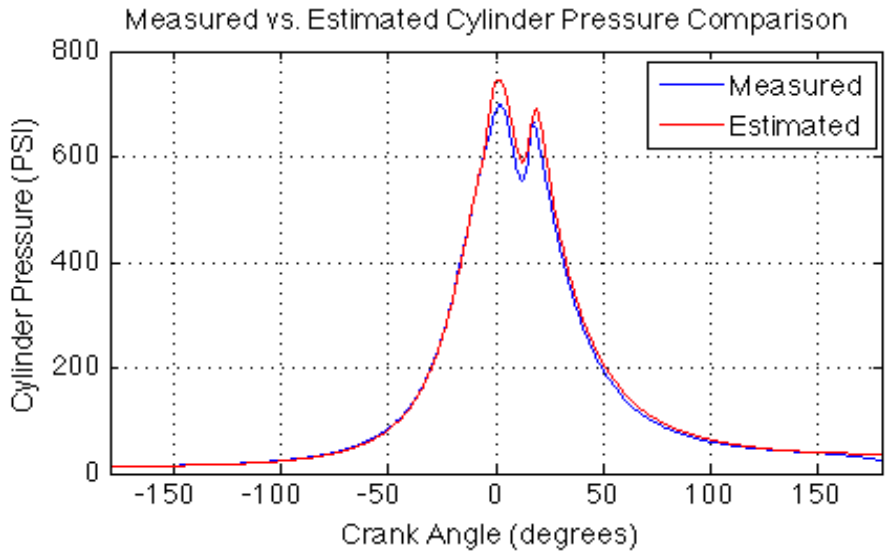

Figure 6 - 5: Measured vs. Estimated Pressure Comparison for 2250 RPM and 62.5% Load

The overestimation of the pilot injection can be seen in the net heat release rate comparison, in Figure 6-6. The estimation seems to be weighted more towards the pre-mixed phase in the pilot injection. Both the pre-mixed and diffusion phases of the main injection match very well with the curve calculated from the measured pressure.

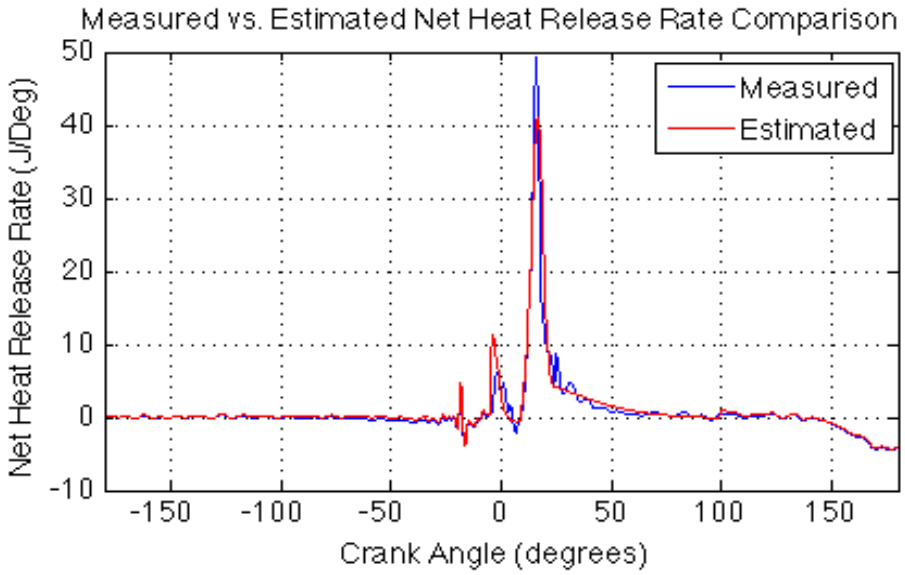

Figure 6 - 6: Net Heat Release Rate Comparison for 2250 RPM and 62.5% Load

The temperature comparison can be seen in Figure 6-7. The overestimation of the pilot injection seems to have an effect on the estimated peak temperature at the main combustion.

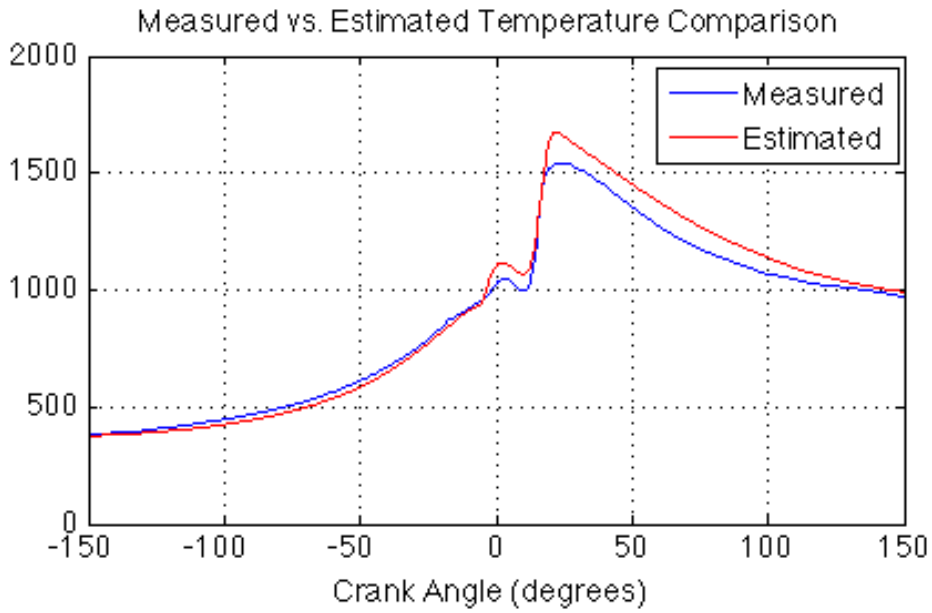

Figure 6 - 7: Temperature Comparison for 2250 RPM 62.5% Load

A similar trend is present between the estimated and measured cumulative gross heat release, shown in Figure 6-8. The separation first becomes present at the pilot injection and only seems to grow slightly during the main combustion. The difference stays constant during expansion. There seems to be little difference between the estimated and measured heat loss to the cylinder. The overall cycle measurements can be seen in Table 6-1. The overestimation of cylinder pressure leads to higher estimated values of indicated work, IMEP, indicated torque, and ISFC.

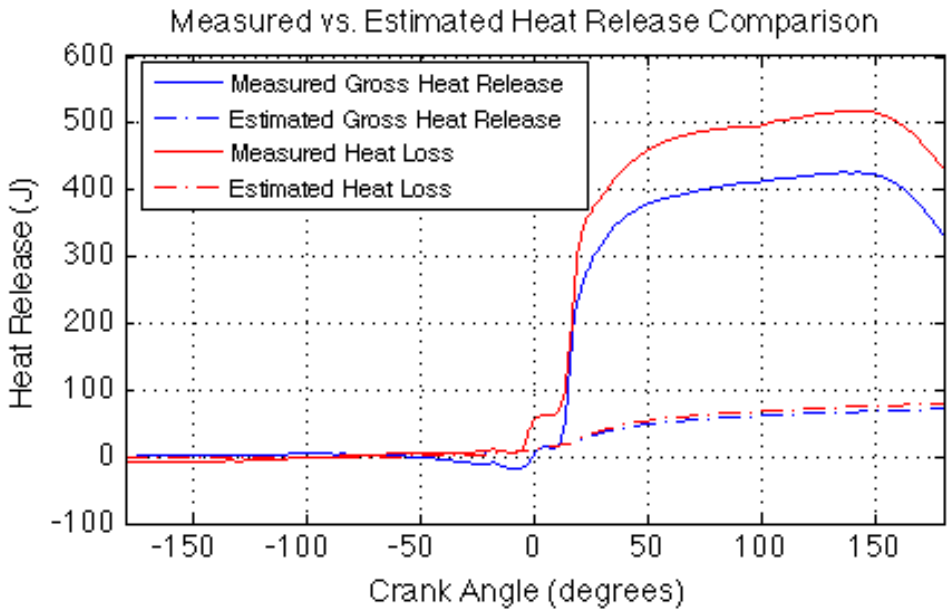

Figure 6 - 8: Cumulative Heat Release Comparison at 2250 RPM 62.5%

Measurement	Value	Estimated
Indicated Work	145.61 lb-ft	166.15 lb-ft
IMEP	76.67 PSI	87.48 PSI
Indicated Torque	34.75 lb-ft	39.64 lb-ft
Dynamometer Torque	26.99 lb-ft	26.99 lb-ft
ISFC	0.3505 lbm/hp·h	0.3072 lbm/hp·h

Table 6 - 1: Cycle Measurements Comparison at 2250 RPM and 62.5% Load

Chapter 7: Conclusions

The goal of this project is to develop a diesel engine test stand that can monitor and record operating conditions while being given a specific load and operating speed. The engine operating parameters are measured at a wide range of sampling rates. This range varies from fractions of a millisecond (cylinder pressure) to multiple seconds (fuel consumption). The programming, physical application, and integration of the variety of sensors with the engine and the computer programs required significant effort and planning. The significant output metrics include operating temperatures (ECT, EGT, oil, intake air, and intercooler), fuel and air mass flow rates, brake torque from the dynamometer, intake manifold and fuel rail pressure values, and the air-fuel ratio. The test stand also has the ability to monitor cylinder pressure, injector current, and fuel rail pressure on a crank angle basis. The end result is a setup that combines the engine, dynamometer, sensors, and LabVIEW to give the user total control operating, monitoring, recording, and processing a wide range of test conditions.

The second part of the project is the development of a series of engine model programs that can create and analyze energy release curves on a crank angle basis. The experimental pressure analysis program outputs the test cylinder pressure, injector current signal, and fuel rail pressure values over a specific crank period. The program can generate P-V diagrams, gross heat release rate, net heat release rate, and heat loss rate curves based on the experimental pressure data. Cumulative gross heat release, net heat

release, and heat loss curves can also be created. The program can also output overall cycle metrics like indicated work, indicated torque, IMEP, and ISFC. A heat release rate approximation model has been created and calibrated based on the outputs of the experimental pressure analysis program for a set of test conditions. The ultimate goal is to be able to use this heat release rate approximation model for a wide range of conditions without the requirement of cylinder pressure data.

The contribution to this project is a reliable engine test stand that is capable of generating the necessary information to analyze combustion based on the fuel and test conditions. The heat release rate approximation model provides a solid foundation which still needs to be improved before it is considered a reliable stand-alone engine model. More investigation into the effects of other control parameters, such as VGT maps, will give a wider perspective of all the influences on combustion. A controllable ECU would allow the user to set these input values, which would become input values in the heat release estimation model. This method gives a quick and reliable way to analyze the effects of additional control parameters on combustion. A better understanding of the control parameter influence will lead to better engine control over varying loads and conditions. The current test stand has been designed to capture the effects of combustion with the available sensors, and the ability to expand for enhancements later in the project. The Matlab programs have the ability to process all available data and analyze their effects on the combustion process.

References

1. Tatsuo Takaishi et al., *Approach to High Efficiency Diesel and Gas Engines*, Mitsubishi Heavy Industries Technical Review Vol.45 No.1 (2008)
2. Green Car Congress blog. *European Automobile Production Grows by 5.3% in 2007; Diesel Accounts for 53.3% of New Car Registrations*. http://www.greencarcongress.com/2008/02/european-automo.html.
3. Heywood, J.B., *Internal Combustion Engine Fundamentals*, 1988, New York, NY: McGraw-Hill, Inc.
4. Rakopoulos, C.D. and Giakoumis, E.G. *Diesel Engine Transient Operation: Principles of Operation and Simulation.* 2009 Springer-Verlog, Berlin.
5. Pulkrabek, Willard W. *Engineering Fundamentals of the Internal Combustion Engine*, 1997, Upper Saddle River, NJ: Pearson Prentice-Hall.
6. G. Woschni and F. Anisits. "Experimental Investigation and Mathematical Presentation of Rate of Heat Release in Diesel Engines Dependent upon Engine Operating Conditions". SAE 740086, 1974.
7. Watson, N., D.A. Pilley, and M. Marzouk, *A Combustion Correlation for Diesel Engine Simulation*. 1980, Society of Automotive Engineers, Inc. p. 51-63.
8. Woschni, G., "A Universally Applicable Equation for the Instantaneous Heat Transfer Coefficient in the Internal Combustion Engine," SAE paper 670931, 1967
9. Assanis, D. N., Filipi, Z. S., Fiveland, S. B., Syrimis, M., *A Methodology for Cycle-By-Cycle Transient Heat Release Analysis in a Turbocharged Direct Injection Diesel*

Engine, SAE Special Publication Series volume SP- 1530, also 2000 SAE Transactions, Journal of Engines, Vol. 109, Section 3, pp. 1327-1339

10. Kim, Chung-Gong. *A Crank Angle Resolved CIDI Engine Combustion Model with Arbitrary Fuel Injection for Control Purpose*. PhD diss., Ohio State University.
11. Olikara, Cherian and Borman, Gary L., "A Computer Program for Calculating Properties of Equilibrium Combustion Products with Some Applications to I.C. Engines," SAE paper 750468, 1975.
12. Buttsworth, David R. (2002) *Spark ignition internal combustion engine modeling using Matlab*. Technical Report. University of Southern Queensland, Faculty of Engineering and Surveying, Toowoomba, Australia.
13. Zawistowski, Thomas and Shah, Paras. *An Introduction to Sampling Theory*, http://www2.egr.uh.edu/~glover/applets/Sampling/Sampling.html.
14. Lancaster D. R., Krieger R. B., and Lienesch J. H.. *Measurement and Analysis Of Engine Pressure Data*. 1975. SAE Technical Paper 750026.
15. "The Piezoelectric Effect, Theory, Design, and Usage", http://www.designinfo.com/kistler/ref/tech_theory_text.htm, Winterthur, Switzerland, Kistler Instrument Corporation
16. "Zero-phase digital filtering." http://www.mathworks.com/help/toolbox/signal/filtfilt.html, Matlab HELP. Mathworks, Inc.

Appendix

Recorded Values for Combustion Analysis

The following table lists the necessary inputs for combustion analysis and how they are obtained:

RPM – Mean Operating Parameter Recording Program	**Brake Torque -** Mean Operating Parameter Recording Program
IMAP - Mean Operating Parameter Recording Program	**MAF -** Mean Operating Parameter Recording Program
Fuel Rail Pressure – Crank Angle Based Recording Program	**Injector Delay –** Calculated from Eq. (5.3)
ECU Pilot and Main Injection Timing (SOI,EOI) - Crank Angle Based Recording Program	Estimated Pilot and Main Injection Fuel Mass – Calculated from Eq. (5.2)
Pilot SOC – Visually determined from cylinder pressure trace output from Experimental Pressure Analysis Program	**Main SOC** – Visually determined from net heat release rate output from Experimental Pressure Analysis Program
Estimated Trapped Air – Calculated from Eq. (3.23) and Mean Operating Parameter Recording Program	**Total Equivalence Ratio -** Mean Operating Parameter Recording Program

List of Simulation Programs

1. constants.m

Defines geometry constants, Woschni heat transfer properties, fuel properties, initial conditions (pressure, temperature, residual equivalence ratio, engine speed), model tolerance.

2. [thetafull,motorpressure,Iavg,Ravg]=fullimport(filtval)

This program imports the measured array excel files recorded from the crank angle based LabVIEW recording program. Once a reduced frequency is chosen, the adjusted cylinder pressure, injector current, and fuel rail pressure vectors are processed based on the method described in Section 4.5. The P-V and log P-V diagrams are also generated.

input: filter reduced frequency
output: average, filtered cylinder pressure; average injector current and fuel rail pressure

3. finalprog.m

This is the top-level program that loads measured fired and motored pressure traces, defines the shape parameters, runs the overall model and experimental pressure analysis program, and calculates overall cycle measurements for comparison.

4.[volset,dQnet1,pprime,dQht1,temp1,netheat1,heat1,work1]=exppressureprog(pressuredata,refmotoredpressure);

This is the experimental pressure analysis program. Once the fired and motored pressure traces are inputted, the volume, net heat release rate, pressure, heat loss rate, temperature, work, and cumulative heat loss and net heat release are calculated as shown in Figure 4.29.

input: fired and motored pressure traces
output: volume, net heat release rate, pressure, heat loss rate, temperature, work, and cumulative heat loss and net heat release

5.yprime=dptestrates6(theta,Y)

This program represents the set of differential equations that are integrated in exppressureprog using ‘ode45’.

input: crank angle and initial guesses to differential equations
output: set of differential equations including heat transfer rate, work rate, net heat release rate, and differential pressure

6.

```
[degree,pressure,temp,work,heat,grossheat,grossheatrate]=progtest
(modelparams1,modelparams2,theta0,p0,T0)
```

This program is the overall model that can be seen in Figure 6-1.

input: shape parameters for pilot and main injections, initial crank angle, pressure, and temperature

output: crank angle position, estimated cylinder pressure, estimated temperature, work, cumulative gross heat release and heat loss, gross heat release rate and heat loss rate

Recommendations for Test Stand Improvement

In order to reach the goal of a stand-alone engine model, a few of the test stand components will need to be upgraded. A needle-lift sensor should be added to provide accurate fuel injection timing. This model estimates SOI based on the injector current signal and an injector delay correlation. The needle-lift sensor will also provide a better estimate of trapped fuel, and subsequently the trapped equivalence ratio. Once an accurate trapped equivalence ratio is applied, a better estimation of the shape parameter coefficients in Watson's model can be produced. Also, a controllable ECU will allow for a wider range of test conditions and allow for the modification of engine control features like EGR and VGT. The controllable ECU will allow the user to set control parameters like injection timing, EGR, and VGT. All of these control parameters also act as inputs into the engine model. A significant amount of time was spent filtering and adjusting the test data. This model would benefit from reduced noise in the pressure sensor.